


# Sedimentological and carbonate isotope signatures to identify fluvial processes and catchment changes in a supposed impact ejecta-dammed lake (Miocene, Germany)

LINGQI ZENG\* , DAG B. RUGE\*, GÜNTHER BERGER†, KARIN HECK‡, STEFAN HÖLZL‡, ANDREAS REIMER\*, DIETMAR JUNG§ and GERNOT ARP\*

\*Georg-August-Universität Göttingen, Geowissenschaftliches Zentrum, Goldschmidtstrasse 3, Göttingen, 37077, Germany (E-mail: lzens@gwdg.de)

†Sudetenstraße 6, Pleinfeld, Germany

‡Staatliche Naturwissenschaftliche Sammlungen Bayerns - RiesKraterMuseum Nördlingen, Eugene-Shoemaker-Platz 1, Nördlingen, 86720, Germany

§Bayerisches Landesamt für Umwelt, Geologischer Dienst, Hans-Högn-Straße 12, Hof/Saale, 95030, Germany

Associate Editor – Concha Arenas

## ABSTRACT

The identification and distinction of fluvial from lacustrine deposits and the recognition of catchment changes are crucial for the reconstruction of climate changes in terrestrial environments. The investigated drill core succession shows a general evolution from red–brown claystones to white–grey marlstones and microcrystalline limestones, which all have previously been considered as relict deposits of an impact ejecta-dammed lake, falling within the mid-Miocene Climate Transition. However, recent mammal biostratigraphic dating suggests a likely pre-impact age. Indeed, no pebbles from impact ejecta have been detected; only local clasts of Mesozoic formations, in addition to rare Palaeozoic lydites from outside of the study area. Lithofacies analysis demonstrates only the absence of lacustrine criteria, except for one charophyte-bearing mudstone. Instead, the succession is characterized by less diagnostic floodplain fines with palaeosols, palustrine limestones with root voids and intercalated thin sandstone beds. Carbonate isotope signatures of the mottled marlstones, palustrine limestones and mud-supported conglomerates substantiate the interpretation of a fluvial setting. Low, invariant  $\delta^{18}\text{O}_{\text{carb}}$  reflects a short water residence time and highly variable  $\delta^{13}\text{C}_{\text{carb}}$  indicates a variable degree of pedogenesis. Carbonate  $^{87}\text{Sr}/^{86}\text{Sr}$  ratios of the entire succession show a unidirectional trend from 0.7103 to 0.7112, indicating a change of the solute provenance from Triassic to Jurassic rocks, identical to the provenance trend from extraclasts. The increase in carbonate along the succession is therefore independent from climate changes but reflects a base-level rise from the level of the siliciclastic Upper Triassic to the carbonate-bearing Lower to Middle Jurassic bedrocks. This study demonstrates that, when information on sedimentary architecture is limited, a combination of facies criteria (i.e. presence or absence of specific sedimentary structures and diagnostic organisms), component provenance, and stable and radiogenic isotopes is required to unequivocally distinguish between lacustrine and fluvial sediments, and to disentangle regional geological effects in the catchment and climate influences.

**Keywords** Base-level, fluvial sediments, Georgensgmünd Formation, Miocene Ries Crater, non-marine carbonates, stable carbon and oxygen isotopes, strontium isotopes.

## INTRODUCTION

Non-marine sediments, when constituting long-lasting stratigraphic records, form valuable climate archives for the reconstruction of past terrestrial environments. Specifically, lacustrine series provide high-resolution records of temperatures, precipitation and orbital forcing (e.g. Olsen, 1986; Cohen, 2003; Leng & Marshall, 2004; Andrews, 2006). Likewise, climate trends can be deduced from fluvial series and palaeosols, although at a lower time resolution (e.g. Demko *et al.*, 2004; Allen *et al.*, 2014; Opluštil *et al.*, 2015). In any case, a proper identification of the depositional setting as well as local effects of tectonics and catchment changes is required. The distinction between a lacustrine and a fluvial setting for sediments such as fine-grained sandstones, floodplain fines, palustrine limestones and oncolitic tufa, however, is still challenging when surface exposures are limited, only few or isolated drillings are available, or occurrences are relict. Then, the geometry of sedimentary bodies (e.g. Miall, 1985, 1996) cannot be determined, and interpretations rely on sedimentological and palaeontological evidence (e.g. Rust, 1982; Selley, 1992; Reading, 1996; Flügel, 2004).

However, stable and radiogenic isotope signatures of carbonate rocks can provide crucial information with respect to hydrology and catchment, and also help to distinguish between fluvial and lacustrine settings. Strontium isotopes form a useful tool in tracing the provenance of fluids and catchment reconstruction (Faure, 1986). Examples are catchment changes during expansion–contraction lake cycles (Rhodes *et al.*, 2002; Doebbert *et al.*, 2014), differentiation of sub-basins with different catchments (Gierlowski-Kordesch *et al.*, 2008) and changes in the chemical composition of lake tributaries upon erosion of different lithological units (Jin *et al.*, 2009; Pietzsch *et al.*, 2018) or impact ejecta (Arp *et al.*, 2013) in the catchment area. In turn, carbonate  $\delta^{13}\text{C}$  and  $\delta^{18}\text{O}$  data sets from continental series are commonly used for reconstructions of palaeoclimate (e.g. Ekart

*et al.*, 1999; Leng & Marshall, 2004; Andrews, 2006), but also help to constrain hydrological conditions (e.g. Talbot, 1990; Li & Ku, 1997), biological activity (e.g. Thompson *et al.*, 1997), palaeoaltimetry (e.g. Cyr *et al.*, 2005; Rowley, 2007) and diagenetic alterations (e.g. Swart, 2015).

The present isotopic and sedimentological study focuses on the example of the Miocene Georgensgmünd Formation in southern Germany. These deposits have previously been considered as lake deposits (Dorn, 1939) that formed as a result of damming of an ancient river by ejecta from the Ries asteroid impact (Birzer, 1969), immediately north of the Northern Alpine Foreland Basin (NAFB) (Fig. 1). It would be, to the knowledge of the authors, the only supposed impact ejecta-dammed lake on Earth reported in literature.

Dependent on different stratigraphic interpretations (Birzer, 1969; Berger, 2010; Schirmer, 2014), the Georgensgmünd Formation falls into the time range of the pre-Ries-impact Miocene Climatic Optimum (MCO, *ca* 17 to 15 Ma; Zachos *et al.*, 2001) or the following post-Ries-impact mid-Miocene Climate Transition (MMCT, *ca* 15 to 13 Ma; e.g. Methner *et al.*, 2020). However, the pre-impact age of deposits, as indicated by mammal fossils (early MN5, Berger, 2010; see Fig. 2), has been questioned (Schirmer, 2014), and later publications (e.g. Sturm *et al.*, 2015) still assume the existence of an impact ejecta-dammed lake. Hence, the effect of the asteroid impact on the fluvial system in this region is still under debate.

The aim of the study is to clarify the lacustrine versus fluvial nature of these deposits, and their relation to the asteroid impact event. The study investigates how sedimentological criteria can be supplemented by stable and radiogenic isotope data to trace provenance of sediments and fluids (from local and distant bedrocks) and disentangle regional factors (base-level changes/tectonics and headwater erosion) and climatic factors controlling sedimentation, when information on sedimentary architecture is limited.

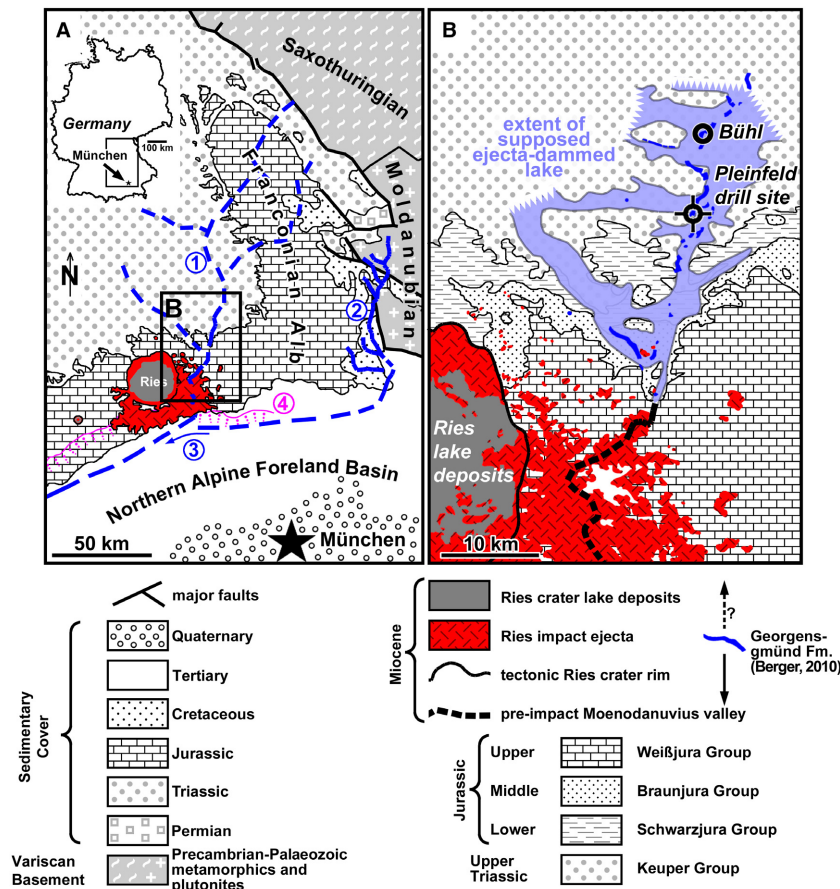


**Fig. 1.** Geographical and geological overview of the study area (based on Freudenberger, 1996). (A) South German Scarplands, with the Ries impact structure and adjacent Northern Alpine Foreland Basin (NAFB). Blue dashed lines indicate the early to middle Miocene south-directed drainage system. Both, ‘the ‘Moenodanuvius’ (1) (Schirmer, 2014) and the ‘Paleonaab’ (2) (Bader *et al.*, 2000), discharge into the ‘Graupensand river’ (3) (Doppler *et al.*, 2002; Pippèr & Reichenbacher, 2017), which drains farther west (finally ending in the westernmost NAFB). The magenta line and dots (4) indicate the cliff line of the early Miocene Upper Marine Molasse (early Otnangian), which is used as a reference for late tectonic tilting (Gall, 1974; Freudenberger, 1996; Doppler *et al.*, 2002). Note the Variscan basement high (Saxothuringian domain and Moldanubian domain) in the north-east. (B) Detail showing the outline of the supposed Rezat-Alt Mühl Lake according to Hüttner & Schmidt-Kaler (1999) and Peterek & Schröder (2010), distribution of the actual sediment relicts of the Georgensgmünd Formation (Berger, 2010) and their geographic relationship to Ries impact ejecta.

## GEOGRAPHIC AND GEOLOGICAL OVERVIEW

The study area is located in the South German Scarplands (Peterek & Schröder, 2010, and references therein), approximately 100 km NNW of Munich (Fig. 1). In this area, high-grade metamorphics and plutonites of the Variscan basement are covered by a 300 to 600 m thick Permomesozoic sediment series: local volcanics and coarse siliciclastics of the Permian Rotliegend Group (up to 300 m), and Triassic arkoses, sandstones and claystones of the Buntsandstein

(ca 50 m), Muschelkalk (ca 50 m) and Keuper Group (225 m) (Haunschild, 1992; Freudenberger, 1996). The latter is overlain by marine deposits of the Jurassic, which comprise dark grey claystones and shales of the Schwarzjura Group (35 m), brown sandstones, iron oolites and claystones of the Braunjura Group (100 m), and white grey limestones and dolomites of the Weißjura Group (>115 m) (Berger *et al.*, 1971, 1982). Since the Cretaceous, the study area has been subject to subaerial exposure and karstification. During the Cenozoic, intense erosion led to the present-day landscape (Wagner, 1960;

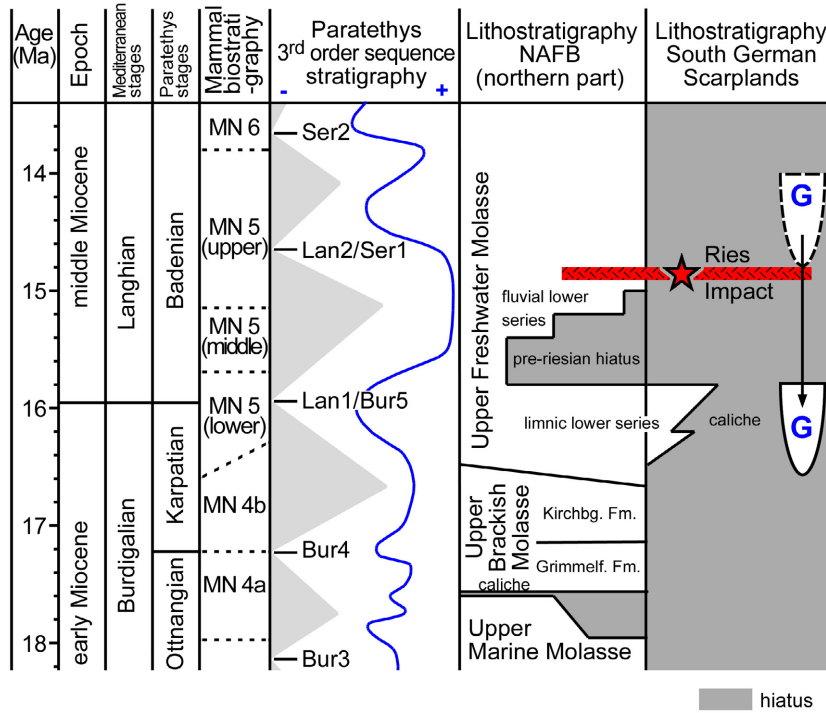


**Fig. 2.** Chronostratigraphy, biostratigraphy and sequence stratigraphy of the Miocene sediment series discussed in this paper. Lithostratigraphy of the Northern Alpine Foreland Basin and the adjacent part of the South German Scarplands according to Doppler *et al.* (2002), Reichenbacher *et al.* (2013) and Pippèr & Reichenbacher (2017). Paratethys sequence stratigraphy and eustatic sea-level curve after Piller *et al.* (2007) and Hardenbol *et al.* (1998), respectively. 'G' indicates the stratigraphic position of the Georgensgmünd Formation suggested by Berger (2013) (solid outline) and previous studies (dashed outline), respectively.

Knetsch, 1963; Hofbauer, 2001; Peterek & Schröder, 2010), however, with an initially southward directed drainage system (i.e. the Moenodanuvius and Paleonaab) (Fig. 1; Peterek & Schröder, 2010; Schirmer, 2014). At 15 Ma, a double asteroid impact event caused the formation of the Ries and Steinheim crater basins, burial of its vicinity by a decametre to 120 m thick ejecta blanket, and subsequent formation of crater lakes (Shoemaker & Chao, 1961; Pohl *et al.*, 1977; for discussion of impact age see Schmieder *et al.*, 2018a,b; Rocholl *et al.*, 2018a, b). Miocene relict deposits of a supposed impact ejecta-dammed lake north-east of the Ries crater basin are the subject of the present study (Fig. 1), because recent biostratigraphic dating points to a likely age older than the impact, consequently leading to questioning of the lacustrine nature of the deposits (Berger, 2010). Herein, the lithostratigraphic name of these Miocene relict deposits is defined as the Georgensgmünd Formation, of which the type locality is a hill ('Bühl') near Georgensgmünd, subject to quarrying at least since the 16<sup>th</sup> century (coordinates: 49°11'49.93" N, 11°0'2.79" E; von Meyer, 1834; Berger, 2010). The region was subject to an epirogenic uplift from 16.5 Ma at near sea-level to the latest Pliocene, leading to present-day altitudes of 360 to 600 metres above sea-

level (m a.s.l.) (Gall, 1974; Hoffmann & Friedrich, 2017; Sant *et al.*, 2017). As a result of the Palaeogene–Neogene erosion, the escarpment of the Franconian Alb, i.e. the Upper Jurassic limestone plateau, is located approximately 8.5 km south-east of the drill site. Top elevations of hills in the vicinity of Pleinfeld still show Lower to Middle Jurassic to marine claystone covers, while slopes and valley floors expose siliciclastics of the Triassic Keuper Group (Berger *et al.*, 1971).

## MATERIAL AND METHODS

The site of the investigated drill core (coordinates: 49°6'58.44" N, 10°58'35.10" E; Berger *et al.*, 1971) is located about 1.3 km north-west of the town Pleinfeld at 412.6 m a.s.l. and lies *ca* 42 m above the water level of the present-day river Rezat (Fig. 1). The obtained drill core is 63 m in length and 5 cm in diameter. The core recovery is 87%, with losses mainly in the lowermost part of the section. The drilling was performed in 1968 by the Bavarian Building Authority for geological site investigation and groundwater observation concerning the establishment of a water reservoir. It is now hosted at the core facility of the Geological Survey at the



Bavarian Environmental Agency in Hof a.d. Saale.

Macroscopic documentation of drill core lithofacies types was carried out using a Sony SLT-A99V camera (Sony Corporation, Tokyo, Japan). For microfacies analysis of carbonates, seven thin sections ( $10 \times 7.5$  cm in size) from the Pleinfeld drill core and 12 thin sections from reference location Bühl near Georgensgmünd were used, with a thickness of 80  $\mu\text{m}$ . The microscopic documentation was carried out by a Zeiss Stemi 2000-C binocular (Carl Zeiss AG, Oberkochen, Germany) equipped with a Canon EOS 500 D camera (Canon Inc., Tokyo, Japan).

Thirty-nine samples were analyzed with respect to their organic ( $C_{\text{org}}$ ) and carbonate carbon ( $C_{\text{carb}}$ ) contents, and stable carbon and oxygen isotope ratios of the carbonate fraction [ $\delta^{13}\text{C}$  and  $\delta^{18}\text{O}$ ; and reported in per mil relative to Vienna Pee Dee Belemnite (V-PDB)]. From the same samples, carbonate for stable carbon and oxygen isotope measurements was obtained under a Zeiss Stemi 2000-C binocular microscope from cut core slabs and hand specimens using a steel needle to sample separate textures. Carbonate powders were reacted with 100% phosphoric acid (density  $>1.95$  g  $\text{cm}^{-3}$ ) at 70°C using a Thermo Kiel IV carbonate preparation line connected to a Finnigan Delta plus mass spectrometer (Thermo Fisher Scientific, Waltham, MA, USA). All values are reported in per mil relative to V-PDB by assigning a  $\delta^{13}\text{C}$  value of +1.95‰ and a  $\delta^{18}\text{O}$  value of -2.20‰ to the NBS 19 standard. Reproducibility was checked by replicate analyses of laboratory standards and is better than  $\pm 0.05\%$  ( $1\sigma$ ). Standard deviations of the stable isotope measurements, if not specifically noted, are 0.05‰ for  $\delta^{13}\text{C}$  and 0.07‰ for  $\delta^{18}\text{O}$ .

Strontium isotope analyses of 26 samples were carried out at the ZERIN, RiesKraterMuseum, Nördlingen, Germany. To specifically dissolve the calcium carbonate fraction, 1 mL of 6N HCl was added to 10 mg of finely ground samples in Teflon beakers and mixed. After 30 s the reactant was pipetted into 1.5 mL containers and centrifuged. While sequential carbonate leaching (Liu *et al.*, 2013; Bellefroid *et al.*, 2018) is required for high-accuracy studies in the context of, for example, recording primary seawater  $^{87}\text{Sr}/^{86}\text{Sr}$  values from bulk samples, the present study aims at resolving trends in a sedimentary setting with weathering solutions from source materials with highly different  $^{87}\text{Sr}/^{86}\text{Sr}$  ratios

(i.e. marine Jurassic carbonate, siliclastics from Variscan basement), and calcite as the sole carbonate mineral phase in the samples. Nonetheless, despite the single-leaching procedure applied here, no correlation between siliciclastic content and  $^{87}\text{Sr}/^{86}\text{Sr}$  ratios was found, neither for 6N HCl leaching nor acetic acid leaching (Table S1), indicating that the  $^{87}\text{Sr}/^{86}\text{Sr}$  variations (0.00091) within the calcite phase between the different samples is much higher than the potential contamination by Sr from the silicate fraction. Indeed, Bailey *et al.* (2000) demonstrated that the application of different methods of dissolution (i.e. water wash, acetic acid, mixed 6N HCl and 6N  $\text{HNO}_3$ ) resulted in errors of up to  $\pm 0.000076$  in  $^{87}\text{Sr}/^{86}\text{Sr}$  in marly chalks. Furthermore, the 6N HCl protocol applied here resulted in systematically lower, not higher,  $^{87}\text{Sr}/^{86}\text{Sr}$  values (by 0.00002 to 0.00036), if compared to results from acetic acid leaching, indicating that these values show the lowest potential contamination by Sr from silicates (with high radiogenic values).

The supernatants of the centrifuged samples were dried and lead to purification and accumulation of Sr, which was achieved using a strontium-specific crown-ether resin [Sr-Spec®; recipe modified from Horwitz *et al.* (1992) and Pin & Bassin (1992)]. Strontium was loaded in a mixture of  $\text{TaCl}_5$ , HF,  $\text{HNO}_3$ ,  $\text{H}_3\text{PO}_4$  and  $\text{H}_2\text{O}$  (Birck, 1986) on single-band tungsten filaments. Strontium isotope ratios were measured in static mode by a thermal ionization mass spectrometer [Thermo Finnigan MAT 261 modified by Spectromat GmbH (Bremen, Germany)]. Measured isotope values were normalized for mass fractionation using the naturally invariant value for  $^{88}\text{Sr}/^{86}\text{Sr}$  of 8.37521 and the exponential fractionation law. Accuracy and precision of the mass spectrometer runs were controlled by analyzing reference material  $\text{SrCO}_3$  NIST SRM 987. During the period of analysis, the measured  $^{87}\text{Sr}/^{86}\text{Sr}$  value was  $0.710218 \pm 0.000014$  (1 SD,  $n = 7$ ). Based on replicate analyses of natural samples the accuracy for the  $^{87}\text{Sr}/^{86}\text{Sr}$  including the complete laboratory procedure is assumed to be better than  $\pm 0.0050\%$  (1 SD). For more details see Köster *et al.* (2018).

Comparing the results of HCl-aliquots and acetic acid-aliquots, equal or lower radiogenic  $^{87}\text{Sr}/^{86}\text{Sr}$  values in the HCl-leachates were found within uncertainties (Table S1). This finding is interpreted as a clear indication that fast HCl-treatment did not mobilize significant amounts of silicate-derived strontium which are expected

to be more radiogenic than the carbonate phase. Thus, it is assumed that the short HCl-leach gives a good approximation of the easily soluble carbonate fraction.

## RESULTS

### Overview of lithofacies succession

The investigated drill core comprises three lithostratigraphic units (Fig. 3). The topmost 1.7 m recovered unconsolidated Quaternary fluvial sands. Between 1.70 m and 48.95 m depth, mixed carbonate–siliciclastic deposits of the Miocene Georgensgmünd Formation were transected. These rocks show a general increase in carbonate content from base to top, associated with change from red–brown to white–grey colours. The base of the Miocene has been positioned at the first occurrence of pebbles derived from the Mesozoic (i.e. a subrounded Jurassic limonite pebble of 2.5 cm diameter at 48.70 m depth). The basal 14 m of the drill core are composed of sandstones and siltstones of the Middle Keuper Group (Carnian–Norian).

### Lithofacies types

Based on carbonate and siliciclastic components, fabric and colour, 10 lithofacies types (LFT) are identified in deposits of the Georgensgmünd Formation from the Pleinfeld drill core and Bühl locality (Figs 4 and 5; Table 1). Organic carbon content of all analyzed lithofacies types is very low (0.04 to 0.09 wt.%), with highest values in LFTs 5 and 7c (0.10 to 0.12 wt.%). Classic lithofacies codes of Miall (1985, 1996) are listed in the table as far as they are equivalent to LFTs from the present study. However, rooted floodplain fines (Fr) of the investigated deposits show a broader spectrum in lithology and fabric so that a more specific denomination by LFTs 7a to 9c is used in this paper.

Generally, the transected sedimentary succession is poor in fossils. Only in LFTs 8 and 9, poorly preserved pulmonate gastropod moulds were found at several depths. One fragment of a long bone at –25.30 m depth (Fig. 6E) is the only vertebrate remain found in the Pleinfeld core. Carbonaceous plant debris was detected in fine-grained sandstones (LFT 4) at –3.55 m depth, and in calcareous marlstone with root voids (LFT 8) at –33.10 m depth.

### Pebble lithofacies

In addition to palustrine limestone pebbles, which have been reworked within the formation (intraclasts), several extraclasts were detected within the drill core succession (see Fig. 6). These extraclasts included:

**1** Five to 10 cm thick intercalations of white–grey, pebbly arkose with angular quartz grains and kaolinized feldspars near the base of the Miocene section (48.90 to 48.95 m and 47.60 to 47.70 m; Fig. 6A) representing a lithology identical to that of the underlying formation. A similar, less coarse-grained arkose clast, about 4 cm in diameter at 39.10 m depth (within LFT 7) belongs to this pebble group too.

**2** Subrounded pebbles, 2 to 5 cm in size, consisting of carbonate-cemented, gravelly, coarse-grained quartz sandstones were found within LFT 7 at 20.05 m, 32.18 m and 39.08 m core depth (Fig. 6B).

**3** Subangular to subrounded, white–grey limestone pebbles, 1.5 to 8.0 cm in size, that occur at 32.30 m, 35.86 m, 37.08 m, 39.04 m and 39.40 m within LFT 7 (Fig. 6B). In thin section, pisoid fragments, coarsely laminated crusts and root voids within a clotted microcrystalline matrix are evident (Fig. 6C).

**4** Several subrounded limonite and siderite clasts between 1.5 cm and 2.5 cm in size were detected in the section at 29.25 m, 38.42 m and 48.60 m depth (Fig. 6D). In addition, a limonite-cemented fine-grained sandstone pebble, 3.5 cm in size, showing a bivalve imprint, was found at 5.10 to 5.20 m depth.

**5** One angular lydite pebble was observed at 46.4 m depth. The 0.5 cm sized pebble is composed of black chert and white quartz fissures.

### Stable carbon and oxygen isotopes

All analyzed carbonates of the investigated drill core and reference samples are calcitic. In general, Miocene carbonates of the Pleinfeld core show a wide range in  $\delta^{13}\text{C}$  from –7.38 to +2.27‰, at a rather limited range in  $\delta^{18}\text{O}$  from –5.48 to –4.16‰ (Fig. 7; Table 2). Indeed,  $\delta^{18}\text{O}$  values neither differ significantly between lithofacies types nor along the core depth (mean value  $\delta^{18}\text{O} = -4.94 \pm 0.31\text{‰}$ ). On the other hand,  $\delta^{13}\text{C}$  values of microcrystalline matrix and nodules in the different lithofacies types (LFTs 4, 7, 8, 9a) show a significant trend (Fig. 7).

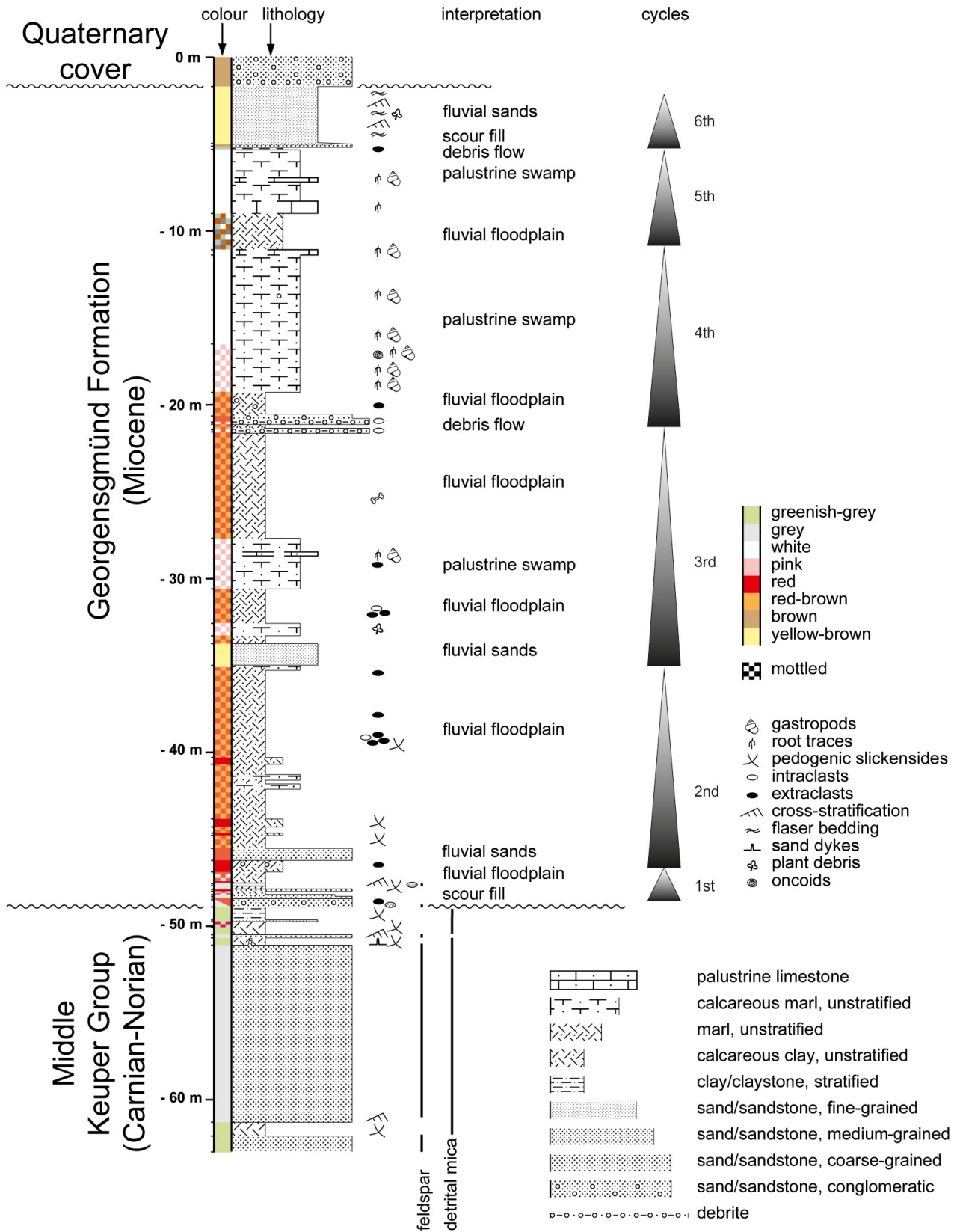


**Fig. 3.** Log of the Miocene Georgensmünd Formation, the underlying Upper Triassic Keuper Group and the overlying Quaternary cover deposits of the Pleinfeld drill core.



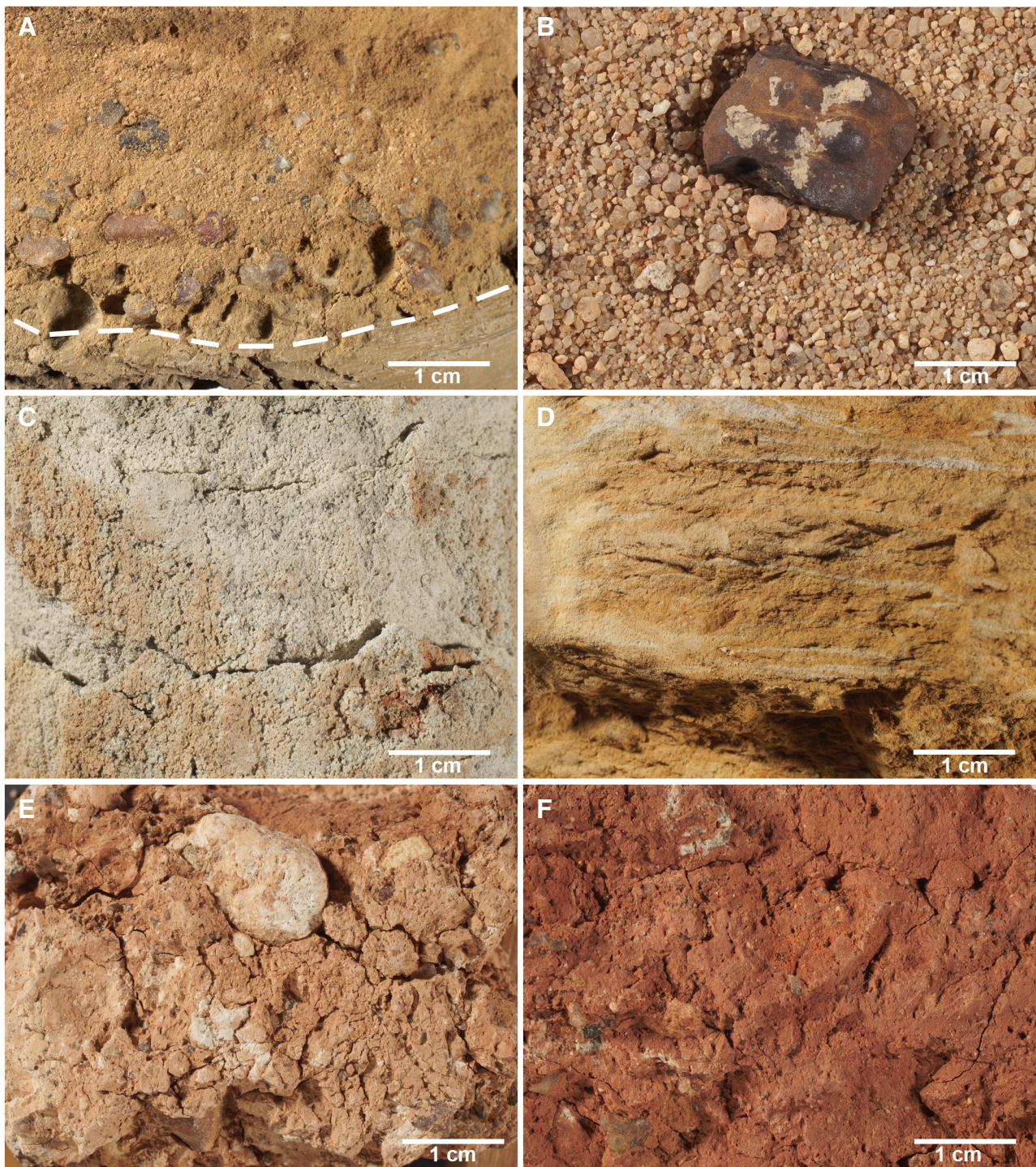


**Fig. 4.** Lithofacies types of the Georgensgmünd Formation. (A) Brown sandy conglomerate/LFT 1 overlaying olive grey claystone/LFT 5 (below the dash line) at 5.10 m core depth. (B) Brown pebbly coarse-grained quartz sand/LFT 2 at 48.64 m core depth, with limonite pebble. (C) Greenish-grey medium-grained quartz sandstone/LFT 3 at 48.25 m core depth. (D) Yellow-brown fine-grained quartz sandstone/LFT4 at 2.30 m, with low-angle cross-stratification. (E) Vari-coloured mud-supported conglomerate LFT 6 at 21.10 m core depth. The white grey pebble is a reworked palustrine limestone. (F) Intense red-brown mottled mudstone LFT 7a at 46.50 m core depth. Note millimetre-sized subangular quartz grains reworked from Keuper arkoses.



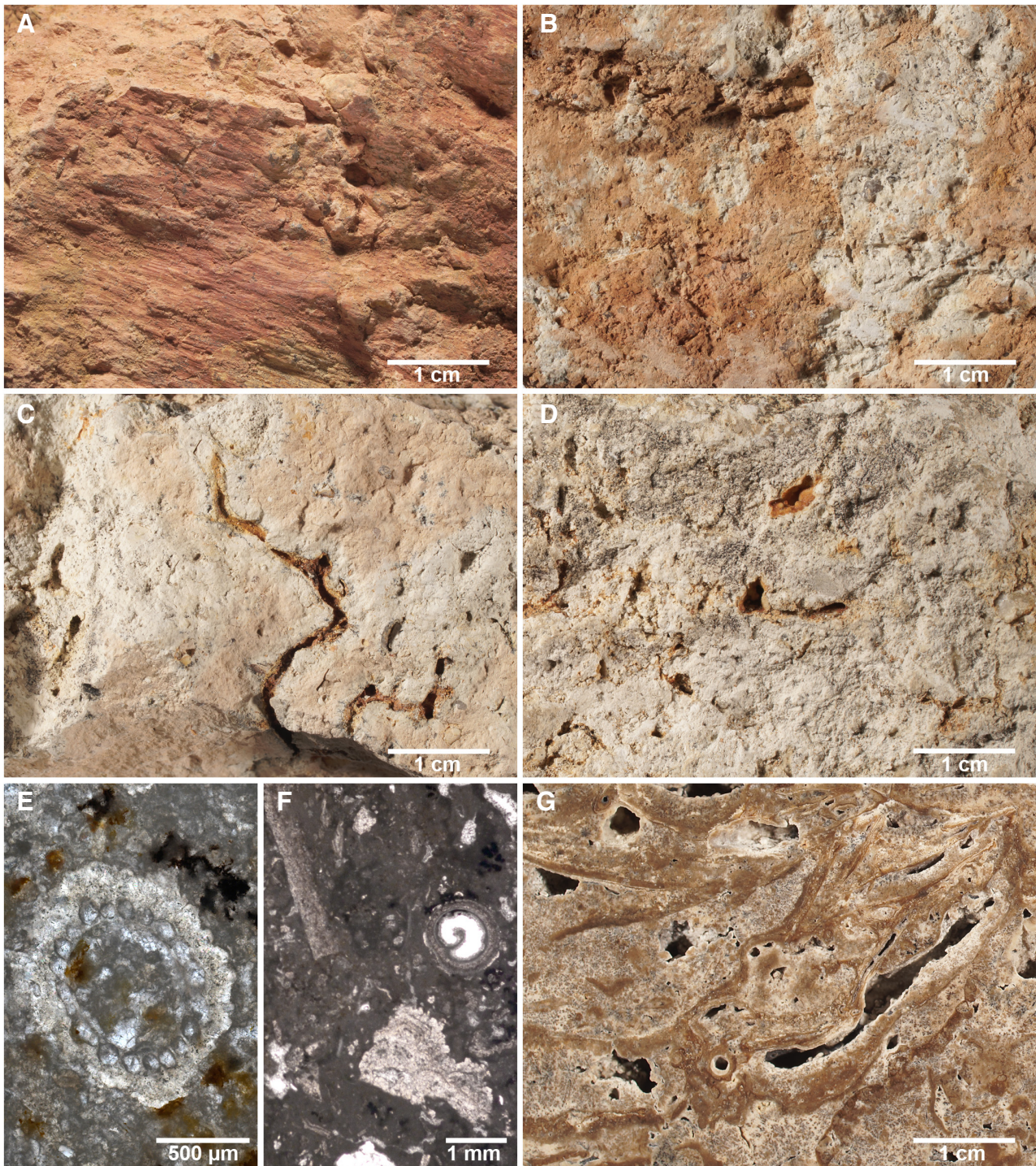


**Fig. 5.** Lithofacies types of the Georgensgmünd Formation. (A) Pedogenic slickensides in intense red-brown mottled mudstone LFT 7a at 39.10 m core depth. (B) Light red-brown mottled mudstone LFT 7b at 22.10 m core depth, with white-grey carbonate patches. (C) Pink-white-grey calcareous marlstone LFT 8 with root voids at 17.40 m core depth. (D) White-grey limestone with root voids LFT 9 at 8.40 m core depth. (E) Thin section microphotograph (transmitted light) of white-grey limestone with charophyte remains LFT9b, at Bühl near Georgensgmünd, Sample GGM 3. (F) Thin section microphotograph (transmitted light) of white-grey limestone with angular tufa fragments LFT 9c and one cement-encrusted hydrobiid gastropod, at Bühl near Georgensgmünd, Sample GGM 4. (G) Polished slab of vacuolar tufa LFT 10, at Bühl near Georgensgmünd, Sample GGM 1.



**Table 1.** Lithofacies types of sediments present in the Miocene Geogensgümd Formation from the Pleinfeld drill core and samples from Bühl.

LFT	Lithofacies	Description	Interpretation	Facies code (Miall, 1985, 2006)	Carbonate content (wt.%)	Thickness (m)
1	Sandy conglomerate	The light-brown conglomerate is composed of well-rounded quartz pebbles up to 1 cm Ø, embedded within fine-grained to coarse-grained quartz sand. Grain-size distribution is fining-upward (Fig. 4A). Quartz pebbles are subangular to poorly rounded.	Fluvial sands	Ss	0	0.05
2	Pebbly coarse-grained sand	This brown coloured, coarse-grained sand shows quartz pebbles up to 5 mm diameter (Fig. 4B). Due to disintegration by the drilling process, no information on sedimentary structures are available.	Fluvial sands	St, Sr, Ss	0	0.4
3	Medium-grained sandstone	Grain size is dominated by medium quartz sand, with a minor argillaceous as well as coarse-grained component. Colour is commonly greenish-grey, but red-brown colours occur as well (Fig. 4C). Similar to the LFTs mentioned above, no carbonate has been detected.	Fluvial sands	St, Sr	0	0.1 to 0.7
4	Fine-grained sandstone	This fine-grained, yellow-brown sandstone is poorly consolidated, rich in silt (Fig. 4D), and locally contains carbonaceous plant debris (e.g. at 3.55 m depth). CaCO <sub>3</sub> content is low, except at the contact to overlying marlstones. Two varieties were recognized: LFT 4a is characterized by a low-angle cross-stratification. LFT 4b shows discontinuous clay laminae reminiscent of flaser bedding.	Fluvial sands	Sr, Sl	<0.1	1.25 to 3.35
5	Clay with pebbles	The olive-grey clay (Fig. 4A) exhibits centimetre-sized limonite sandstone pebbles derived from the Jurassic (Eisensandstein Formation). Scattered quartz pebbles are floating in the clay matrix. No stratification is evident.	Debris flow	Gmm	0.2	0.1 to 0.15
6	Mud-supported conglomerate	Major components (Fig. 4E) are subrounded quartz (up to 9 mm diameter) and palustrine limestone pebbles (up to 4 cm diameter). These pebbles float in a red-brown to white-grey mottled, argillaceous to arenaceous matrix.	Debris flow	Gmm	34 to 44	0.07 to 0.1

Table 1. (continued)

LFT	Lithofacies	Description	Interpretation	Facies code (Miall, 1985, 2006)	Carbonate content (wt.%)	Thickness (m)
7a	Mottled mudstone	Intense red-brown, massive mudstone with pedogenic slickensides (Figs 4F and 5A) and millimetre-sized quartz pebbles.	Floodplain	Fm	0.1 to 6.5	0.15 to 5.3
7b	Mottled mudstone	Light red-brown mottled mudstone, with millimetre-sized quartz pebbles and white-grey carbonate nodules (Fig. 5B).	Floodplain with pedogenic carbonate precipitation	Fm	0 to 63	0.10 to 6.25
7c	Mottled mudstone	Vari-coloured (white-brown-grey) mottled mudstone with millimetre-sized quartz pebbles.	Floodplain with pedogenic carbonate precipitation	Fm	17 to 56	0.17 to 2.1
8	Calcareous marlstone	This lithofacies has a white-grey to pale-pink colour. Abundant yellowish root voids (Fig. 5C) are preserved as well as shell fragments of pulmonate gastropods. Dispersed quartz grains up to 5 mm diameter are also common; locally, the isolated and rounded quartz pebbles have a size up to 1 cm diameter. Except rare intercalated light-olive grey clay layers, no evident stratifications are shown. CaCO <sub>3</sub> content varies between 54 and 74 wt.%, with lower content upon olive grey clay intercalations (31 wt.%).	Palustrine swamp	Fr	54 to 74	0.7 to 5.1
9a	Limestone	White-grey microcrystalline limestone with abundant root voids (Fig. 5D), mud-supported fabric.	Palustrine swamp	Fr	85 to 93	0.3 to 3.8
9b	Limestone	White-grey microcrystalline limestone with charophytes, poor in root voids (Fig. 5E), mud-supported fabric.	Pond	Fr	85 to 93	0.3 to 3.8
9c	Limestone	White-grey limestone with oncoïd fragments, poor in root voids, mud-supported to grain-supported fabric.	Marginal pond	Fr	85 to 93	0.3 to 3.8
10	Vacuolar tufa	This lithofacies represents a mixture of grey phytoclastic and framestone tufa (Manzo <i>et al.</i> , 2012; Fig. 5G). The tufa is a porous but solid-framed limestone composed of undulating horizontal 5 mm thick calcite sheets (probably encrusted leaves), peloidal fabric and laminoid fenestrae. Pulmonate gastropods were locally observed. CaCO <sub>3</sub> content can be high (not analyzed).	Freshwater spring or small tufa barrage	[n.a.]	[n.a.]	[n.a.]

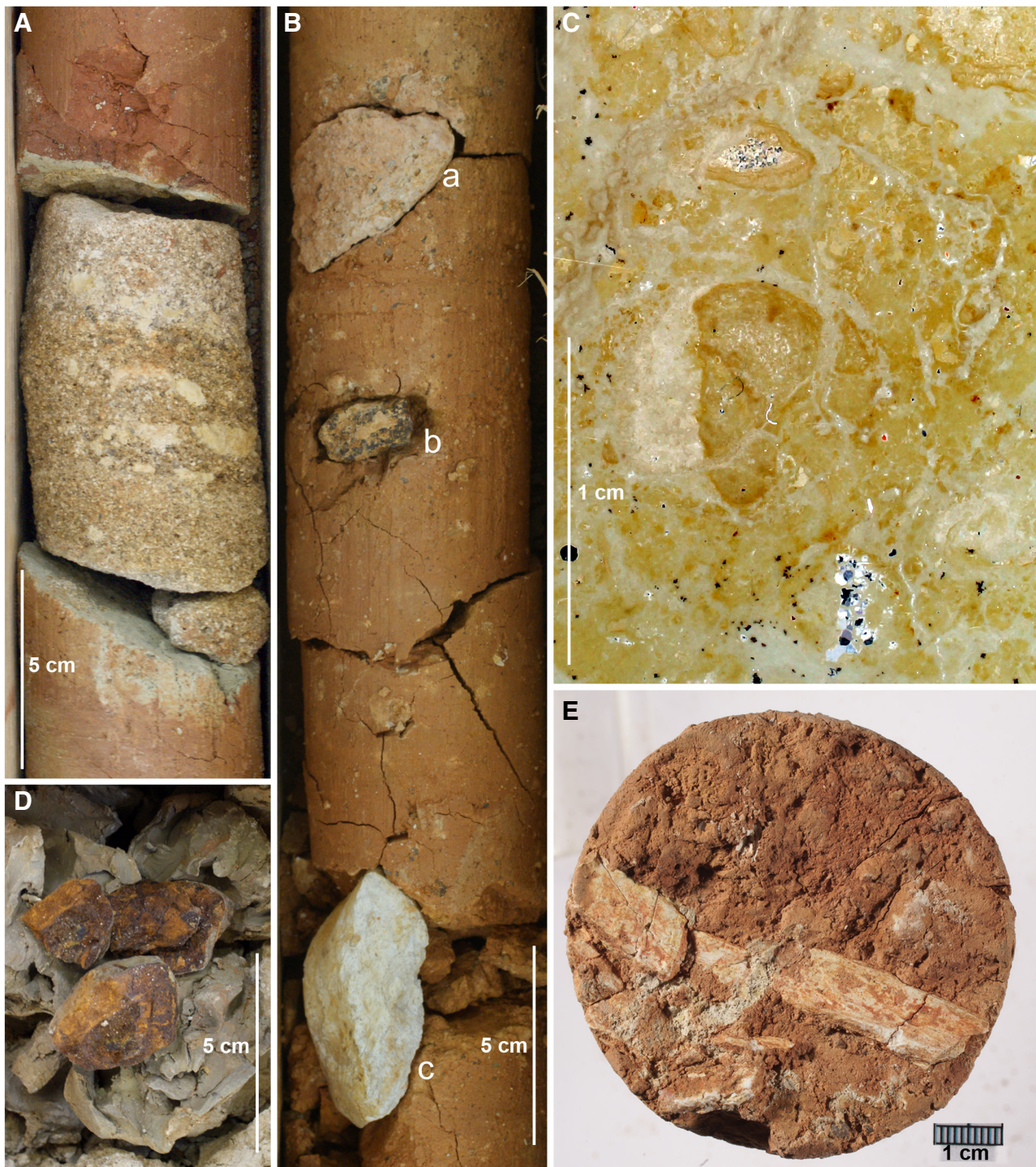


**Fig. 6.** (A) Pleinfeld drill core at 47.55 to 47.75 m depth showing a 10 cm arkose intercalation (i.e. a cobble) of Upper Triassic origin, between Miocene mottled mudstones. (B) Drill core at 32.05 to 32.35 m depth showing a pink–white–grey limestone pebble ('a' 32.10 m), a sub-angular manganese-oxide-stained Arietensandstein pebble ('b' 32.18 m) and a subrounded caliche pebble reminiscent of Upper Jurassic marine limestone ('c' 32.30 m). (C) Thin section microphotograph (transmitted light) of the caliche pebble at 32.30 m core depth, showing laminar crusts and *in situ* cracked components. (D) Limonitic sandstone pebble (fragmented) in olive grey claystones of LFT 5 at 5.15 m core depth. (E) Fragmented long bone within light red-brown mottled mudstone of LFT 7b at 25.40 m core depth.



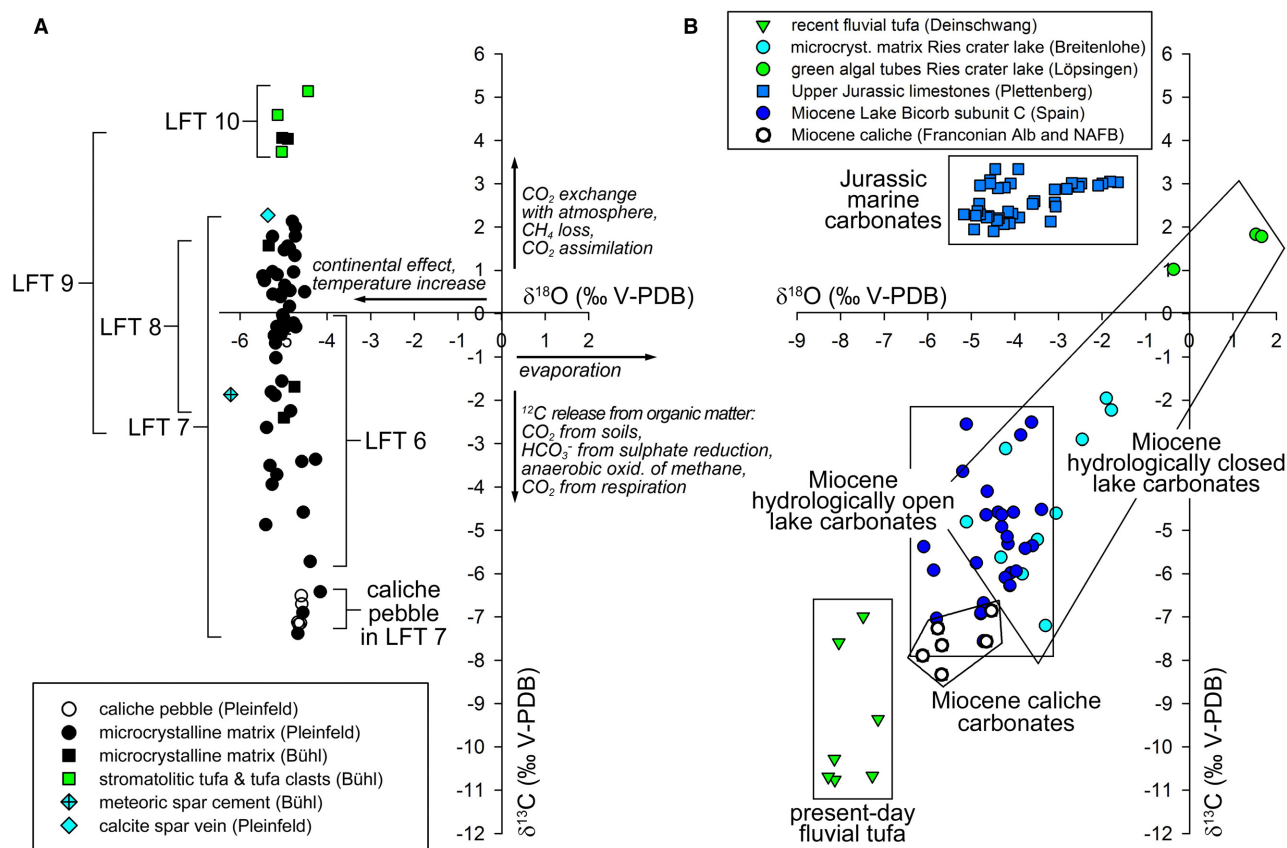


**Fig. 7.** (A) Covariation plot of stable carbon and oxygen isotopes of the carbonate samples in different lithofacies from Georgensgmünd Formation (drill core from Pleinfeld and outcrop from Bühl, this study). (B) Covariation plot of stable carbon and oxygen isotopes of reference material. Miocene caliche carbonates from the Franconian Alb (Hofstetten, Langenthalheim) and NAFB (Burgau), the Miocene Ries impact crater lake carbonates (Arp *et al.*, 2017a,b), the Miocene Lake Bicorn subunit C (Spain; Utrilla *et al.*, 1998), Upper Jurassic marine limestone (Southern Germany; Ruf *et al.*, 2005), and present-day fluvial tufa (Franconian Alb; Arp *et al.*, 2001).

Lowest  $\delta^{13}\text{C}$  average values ( $\delta^{13}\text{C} = -6.93 \pm 0.30\text{‰}$ ) were obtained from a reworked caliche pebble in LFT 7. The carbonate matrix and nodules in LFT 7 revealed a wide range in  $\delta^{13}\text{C}$  but show the lowest value ( $-7.38\text{‰}$ ) and average ratios ( $-1.99 \pm 2.91\text{‰}$ ). Reworked material of this lithofacies type in LFT 6 have a similar wide range ( $-2.75 \pm 2.96\text{‰}$ ). Increasing  $\delta^{13}\text{C}$  values were obtained from LFT 8 (mean:  $-0.55 \pm 1.47\text{‰}$ ) and highest  $\delta^{13}\text{C}$  values were found in palustrine limestone LFT 9a (mean:  $+0.77 \pm 0.65\text{‰}$ ).

Further single measurements fit into this framework: One value obtained from microcrystalline carbonate in the LFT 4 sandstone ( $\delta^{13}\text{C} = -1.89\text{‰}$ ) is close to values in LFT 7. One gastropod shell in LFT 9a shows a  $\delta^{13}\text{C}$  of  $+0.96\text{‰}$ , i.e. within range of host rock LFT 9a. The bone remains in LFT 7 exhibit a  $\delta^{13}\text{C}$  of  $-3.71\text{‰}$ , again within range of host rock. The diagenetic

calcite spar vein ( $\delta^{13}\text{C} = +2.27\text{‰}$ ) in LFT 7 is close to the maximum values in its host rock.

Nine reference isotope analyses have been carried out on carbonates of the Georgensgmünd Formation from Bühl near Georgensgmünd; the  $\delta^{13}\text{C}$  values of the microcrystalline matrix of palustrine limestones LFT 9a are similar to that of palustrine limestones in the Pleinfeld core. The matrix of charophyte and oncid bearing LFT 9bc already shows increased, positive  $\delta^{13}\text{C}$  values, exceeding Pleinfeld palustrine limestone LFT 9a. Very high  $\delta^{13}\text{C}$  values up to  $+5.14\text{‰}$  were obtained from stromatolitic and oncid fragments (LFT 10). Likewise, the  $\delta^{18}\text{O}$  of matrix and components mentioned above is within the same narrow range (mean:  $-4.95 \pm 0.27\text{‰}$ ) as the Pleinfeld carbonates. The diagenetic spar cement in LFT 10 (Fig. 7A) is, with respect to its  $\delta^{13}\text{C}$  ratio, within the range of palustrine carbonates ( $\delta^{13}\text{C} =$

**Table 2.** Carbonate stable oxygen and carbon isotope ratios, and carbonate content of the Pleinfeld drill core (PF) and Bühl (GGM) samples from the Miocene Geogensgünd Formation. Standard deviations of the stable isotope measurements, if not specifically noted, are 0.05‰ for  $\delta^{13}\text{C}$  and 0.07‰ for  $\delta^{18}\text{O}$ .

Sample number	Depth (m)	Lithofacies description	Lithofacies type	Analyzed material	$\delta^{13}\text{C}$ (‰ V-PDB)	$\delta^{18}\text{O}$ (‰ V-PDB)	CaCO <sub>3</sub> (wt.%)
PF10	5.7	White-grey limestone with root voids	9	Microcrystalline matrix (calcite)	0.65	-4.97	53.72
PF10	5.7	White-grey limestone with root voids	9	Microcrystalline matrix (calcite)	0.45	-5.24	53.72
PF12	6.7	White-grey calcareous marlstone with root voids	8	Microcrystalline matrix (calcite)	1.34	-4.74	31.27
PF12	6.7	White-grey calcareous marlstone with root voids	8	Microcrystalline matrix (calcite)	1.51	-4.87	31.27
PF15	7.5	White-grey limestone with root voids	9	Microcrystalline matrix (calcite)	1.99	-4.73	84.51
PF15	7.5	White-grey limestone with root voids	9	Algal carbonate tube (calcite)	1.56	-4.9	84.51
PF16	8.0	White-grey limestone with root voids	9	Microcrystalline matrix (calcite)	0.97	-5.25	54.67
PF17	8.4	White-grey limestone with root voids	9	Microcrystalline matrix (calcite)	1.47	-4.98	92.53
PF21	9.0	White-grey limestone with root voids	9	Microcrystalline matrix (calcite)	0.9	-5.15	91.01
PF21	9.0	White-grey limestone with root voids	9	Gastropod shell fragment (calcite)	0.96	-4.77	91.01
PF22	9.3	Vari-coloured mottled marlstone	7c	Microcrystalline matrix (calcite)	2.13	-4.8	16.64
PF22	9.3	Vari-coloured mottled marlstone	7c	Microcrystalline matrix (calcite)	1.79	-4.73	16.64
PF23*	10.3	White-grey limestone with root voids	9	Microcrystalline matrix (calcite)	-0.31	-4.72	55.68
PF23	10.3	White-grey limestone with root voids	9	Microcrystalline matrix (calcite)	0.5	-4.52	55.68
PF24	11.3	White-grey limestone with root voids	9	Microcrystalline matrix (calcite)	1.78	-5.25	92.52
PF25	12.4	White-grey calcareous marlstone with root voids	8	Microcrystalline matrix (calcite)	-0.48	-5.06	67.32
PF27	14.5	White-grey calcareous marlstone with root voids	8	Microcrystalline matrix (calcite)	-2.25	-4.84	58.12
PF28	15.5	White-grey limestone with root voids	9	Microcrystalline matrix (calcite)	0.17	-4.87	73.99
PF29*	16.8	White-grey calcareous marlstone with root voids	8	Microcrystalline matrix (calcite)	-0.29	-4.92	73.03
PF29*	16.8	White-grey calcareous marlstone with root voids	8	Microcrystalline matrix (calcite)	0.39	-5.07	73.03



Table 2. (continued)

Sample number	Depth (m)	Lithofacies description	Lithofacies type	Analyzed material	$\delta^{13}\text{C}$ (‰ V-PDB)	$\delta^{18}\text{O}$ (‰ V-PDB)	$\text{CaCO}_3$ (wt.%)
PF33*	17.8	Light-pink limestone with root voids	9	Microcrystalline matrix (calcite)	0.47	-5.03	72.58
PF33	17.8	Light-pink limestone with root voids	9	Microcrystalline matrix (calcite)	0.47	-5.04	72.58
PF35	19.0	Light-pink limestone with root voids	9	Microcrystalline matrix (calcite)	0.53	-4.86	72.35
PF37	20.1	Red-brown mottled marlstone	7b	Microcrystalline nodule (calcite)	-0.68	-5.19	34.18
PF37	20.1	Red-brown mottled marlstone	7b	Microcrystalline nodule (calcite)	-0.51	-5.22	34.18
PF38*	21.1	Vari-coloured mud-supported conglomerate	6	Microcrystalline matrix (calcite)	-5.72	-4.39	44.31
PF38	21.1	Vari-coloured mud-supported conglomerate	6	Microcrystalline nodule (calcite)	-0.09	-5	44.31
PF39	21.5	Vari-coloured mud-supported conglomerate	6	Microcrystalline nodule (calcite)	-0.33	-4.97	34.32
PF39	21.5	Vari-coloured mud-supported conglomerate	6	Microcrystalline matrix (calcite)	-4.87	-5.41	34.32
PF40	22.1	Red-brown mottled marlstone	7b	Microcrystalline carbonate streak (calcite)	-1.81	-5.28	43.5
PF41	23.3	Red-brown mottled marlstone	7b	Microcrystalline matrix (calcite)	-3.5	-5.31	35.59
PF43*	25.3	Red-brown mottled marlstone	7b	Microcrystalline matrix (calcite)	-4.58	-4.55	31.52
PF43	25.3	Red-brown mottled marlstone	7b	Calclified bone remains (calcite)	-3.71	-5.16	31.52
PF45	27.2	Red-brown mottled marlstone	7b	Microcrystalline nodule (calcite)	-3.94	-5.26	30
PF46	28.4	Light-pink calcareous marlstone with root voids	8	Microcrystalline matrix (calcite)	-2.63	-5.39	68.63
PF49*	30.2	Light-pink calcareous marlstone with root voids	8	Microcrystalline matrix (calcite)	-1.56	-5.04	59.02
PF49	30.2	Light-pink calcareous marlstone with root voids	8	Microcrystalline matrix (calcite)	-1.02	-5.18	59.02
PF52	32.2	Red-brown mottled marlstone	7b	Microcrystalline nodule (calcite)	-6.42	-4.16	25.72
PF53	32.3	Caliche pebble (found within LFT 7b)	7b	Clotted microcrystalline matrix (calcite)	-6.51	-4.59	n.a.
PF53	32.3	Caliche pebble (found within LFT 7b)	7b	Clotted microcrystalline matrix (calcite)	-7.12	-4.67	n.a.
PF53	32.3	Caliche pebble (found within LFT 7b)	7b	Clotted microcrystalline matrix (calcite)	-6.7	-4.58	n.a.
PF53	32.3	Caliche pebble (found within LFT 7b)	7b	Clotted microcrystalline matrix (calcite)	-7.14	-4.61	n.a.
PF53	32.3	Caliche pebble (found within LFT 7b)	7b	Clotted microcrystalline matrix (calcite)	-7.17	-4.65	n.a.

Table 2. (continued)

Sample number	Depth (m)	Lithofacies description	Lithofacies type	Analyzed material	$\delta^{13}\text{C}$ (‰ V-PDB)	$\delta^{18}\text{O}$ (‰ V-PDB)	$\text{CaCO}_3$ (wt.%)
PF54	33.1	Red-brown mottled marlstone	7b	Microcrystalline matrix (calcite)	-0.22	-4.77	62.61
PF55	34.0	Yellow-brown fine-grained sandstone	4	Microcrystalline carbonate between sand grains (calcite)	-1.89	-5.2	33.55
PF56	35.1	Red-brown mottled marlstone	7b	Microcrystalline carbonate streak (calcite)	-0.03	-5.02	58.79
PF58	37.1	Red-brown mottled marlstone	7b	Microcrystalline matrix (calcite)	-3.41	-4.58	30.78
PF58	37.1	Red-brown mottled marlstone	7b	Microcrystalline nodule (calcite)	-6.9	-4.56	30.78
PF58	37.1	Red-brown mottled marlstone	7b	Microcrystalline nodule (calcite)	-7.38	-4.67	30.78
PF58	37.1	Red-brown mottled marlstone	7b	Microcrystalline carbonate streak (calcite)	-0.3	-5.16	30.78
PF58	37.1	Red-brown mottled marlstone	7b	Microcrystalline carbonate streak (calcite)	-0.37	-5.08	30.78
PF61	39.1	Red-brown mottled marlstone	7b	Microcrystalline matrix (calcite)	0.87	-5.48	47.9
PF63*	41.8	Red-brown mottled marlstone	7b	Microcrystalline matrix (calcite)	-3.36	-4.26	21.43
PF65	43.3	Red-brown mottled marlstone	7b	Microcrystalline carbonate streak (calcite)	0.76	-5.44	60.12
PF65	43.3	Red-brown mottled marlstone	7b	Calcite spar vein	2.27	-5.36	60.12
GGM1	n.a.	Stromatolitic tufa	10	Spar cement (calcite)	-1.87	-6.21	n.a.
GGM1	n.a.	Stromatolitic tufa	10	Stromatolite lamina (calcite)	3.74	-5.04	n.a.
GGM2	n.a.	White-grey limestone with root voids	9	Microcrystalline matrix (calcite)	-1.69	-4.75	n.a.
GGM2	n.a.	White-grey limestone with root voids	9	Microcrystalline matrix (calcite)	-2.4	-4.99	n.a.
GGM3	n.a.	Yellow-grey limestone with charophytes	9	Microcrystalline matrix (calcite)	1.57	-5.34	n.a.
GGM3	n.a.	Yellow-grey limestone with charophytes	9	Microcrystalline matrix (calcite)	4.04	-4.9	n.a.
GGM3	n.a.	Yellow-grey limestone with charophytes	9	Oncoid (calcite)	4.59	-5.14	n.a.
GGM4	n.a.	White-grey limestone with root voids and oncoid clasts	9	Microcrystalline matrix (calcite)	4.06	-5.03	n.a.
GGM4	n.a.	White-grey limestone with root voids and oncoid clasts	9	Oncoid (calcite)	5.14	-4.44	n.a.

Note: the samples marked with \* have standard deviations of 0.08‰ for  $\delta^{13}\text{C}$  and 0.11‰ for  $\delta^{18}\text{O}$ .

−1.87‰) but differs from all other samples by a lower  $\delta^{18}\text{O}$  value ( $\delta^{18}\text{O} = -6.21\text{‰}$ ).

Finally, seven reference values were obtained from early Miocene caliche carbonates (Karpatian and Ottangian) of the Frankenalb and the NAFB. Except for one outlier, the  $\delta^{13}\text{C}$  values of the caliche range from −8.36 to −6.88‰, with an average of  $-7.62 \pm 0.51\text{‰}$ . These values are similar to that of the analyzed caliche pebble in the Pleinfeld core. The  $\delta^{18}\text{O}$  values of the caliche carbonates range from −6.12 to −4.54‰, with an average value of  $-5.41 \pm 0.65\text{‰}$ .

### Strontium isotopes

$^{87}\text{Sr}/^{86}\text{Sr}$  ratios of the carbonate fraction of LFTs 4 and 6 to 9 were analyzed, with all samples showing carbonate content >20 wt.%. In total, the  $^{87}\text{Sr}/^{86}\text{Sr}$  values range from 0.71030 to 0.71121, with a mean value of 0.71065 (Table 3). An almost unidirectional trend of increasing  $^{87}\text{Sr}/^{86}\text{Sr}$  ratios from the base to the top of the section is evident (Fig. 8).

Low  $^{87}\text{Sr}/^{86}\text{Sr}$  values obtained from red–brown mottled mudstones (LFT 7b,  $n = 7$ , 21.4 to 60.1 wt.%  $\text{CaCO}_3$ ) range between 0.71033 and 0.71061 (mean value: 0.71039). A single sample of yellow–brown fine-grained (calcareous) sandstone (LFT 4, 33.6 wt.%  $\text{CaCO}_3$ ) falls in the same range (0.71045), whereas the analyzed sample of vari-coloured mottled mudstone (LFT 7c, 55.7 wt.%  $\text{CaCO}_3$ ) is higher in  $^{87}\text{Sr}/^{86}\text{Sr}$  (0.71085). Light-pink calcareous marlstones with root voids (LFT 8,  $n = 12$ , 31.3 to 74.0 wt.%  $\text{CaCO}_3$ ) show a wide range of  $^{87}\text{Sr}/^{86}\text{Sr}$  values, ranging from 0.71030 to 0.71121 (mean value: 0.71071). White–grey limestone with root voids (LFT 9,  $n = 4$ , 84.5 to 92.5 wt.%  $\text{CaCO}_3$ ) is characterized by high values with low standard deviation (0.71086 to 0.71094; mean value: 0.71090).

A covariation plot of silicate content and  $^{87}\text{Sr}/^{86}\text{Sr}$  ratios indicates that there is no correlation between both parameters (Fig. S1), confirming that there is no or only insignificant leaching of Sr from silicates during sample preparation. Even within LFT 8, i.e. the lithofacies showing the most variable  $^{87}\text{Sr}/^{86}\text{Sr}$ , no covariance can be found between silicate content and  $^{87}\text{Sr}/^{86}\text{Sr}$ .

## INTERPRETATION AND DISCUSSION

### Depositional setting: fluvial or lacustrine?

Early geologists studying the Georgensgmünd Formation were puzzled by the occurrence of

Miocene limestones isolated within the siliciclastic-dominated landscape of the Keuper outcrop (Reck, 1912). Krumbeck (1926, 1927) explained the isolated limestones as karstic spring deposits, which indicated the former position of the Jurassic escarpment. Reck (1912, p. 202) and Wagner (1923), in turn, argued for a lake setting which reflected the damming of a drainage system. This view was supported by Dorn (1939, p. 82) who noted that the freshwater limestones form nodules and thin lenses embedded within claystones and argillaceous marlstones.

The lacustrine interpretation was expanded by Birzer (1969), who suggested that the Georgensgmünd Formation consisted of: "deposits from a lake dammed by the Ries impact ejecta formations onto the Moenodanuvius (Palaeo-Main River) in Franconian Alb area". Consequently, the supposed ejecta-dammed 'Rezat-Alt-mühl-lake' was assigned to a post-Ries-impact age, i.e. Badenian (Berger, 1973; Fischer, 1983). This view persisted until recent times (e.g. Hüttner & Schmidt-Kaler, 1999; Weiss *et al.*, 2008; Peterek & Schröder, 2010; Sturm *et al.*, 2015).

However, Berger (2010) argued that on the basis of mammal teeth fossils [specifically *Anomalomys minor Fejfar*, *Megacricetodon bourgeoisi* (Schaub) and *Galerix exilis* (Blainville)] being present at Bühl (Fig. 1), that the calcareous top parts of the Georgensgmünd Formation belongs to early MN5 (Karpatian), i.e. an age that is probably older than the radiometrically dated Ries impact event (Schmieder *et al.*, 2018a,b:  $14.808 \pm 0.038$  Ma; Rocholl *et al.*, 2018a,b: 14.93 to 15.00 Ma). Indeed, while an accurate radiometric age of the upper boundary of MN5 is available (Krijgsman *et al.*, 1996, Agustí *et al.*, 2001:  $13.75 \pm 0.03$  Ma), the precise age position of its lower boundary (Krijgsman *et al.*, 1996:  $17.26 \pm 0.01$  Ma; Reichenbacher *et al.*, 2013: 16.3 to 16.6 Ma) and subunits (early, middle, late MN5) are less well-established. This biostratigraphic dating, therefore, leads to the question of whether the deposits are related to the Ries impact, and whether they are of lacustrine origin at all.

While the distinction of lacustrine and fluvial sedimentary rocks is facilitated when the three-dimensional geometry of beds is observable, depositional interpretations of relict deposits with limited outcrops and/or isolated drill cores can be ambiguous. For instance, red–brown massive mudstones, can be formed both in lacustrine settings (e.g. Clemmensen *et al.*, 1998) as

**Table 3.**  $^{87}\text{Sr}/^{86}\text{Sr}$  ratio of the carbonate samples from the Miocene Geogensgmünd Formation, reacted with standard 6N HCl. Note that  $2\sigma$  indicates the instrumental precision of measurements.

Sample number	Depth (m)	Sample description	Facies	Analyzed material	$^{87}\text{Sr}/^{86}\text{Sr}$ [6N HCl]	
					Mean	$2\sigma$
PF10	5.70	White-grey calcareous marl with root voids	8	Microcrystalline matrix	0.71121	0.00001
PF12	6.70	White-grey calcareous marl with root voids	8	Microcrystalline matrix	0.71099	0.00002
PF15	7.50	White-grey limestone with root voids	9	Microcrystalline matrix	0.71086	0.00001
PF16	7.95	White-grey calcareous marl with root voids	8	Microcrystalline matrix	0.71093	0.00002
PF17	8.40	White-grey limestone with root voids	9	Microcrystalline matrix	0.71093	0.00002
PF21	8.95	White-grey limestone with root voids	9	Microcrystalline matrix	0.71089	0.00002
PF23	10.33	Vari-coloured mottled mudstone	7c	Microcrystalline matrix	0.71085	0.00001
PF24	11.25	White-grey limestone with root voids	9	Microcrystalline matrix	0.71094	0.00002
PF25	12.40	White-grey calcareous marl with root voids	8	Microcrystalline matrix	0.71086	0.00002
PF27	14.5	White-grey calcareous marl with root voids	8	Microcrystalline matrix	0.71066	0.00002
PF28	15.48	White-grey calcareous marl with root voids	8	Microcrystalline matrix	0.71066	0.00002
PF29	16.75	White-grey calcareous marl with root voids	8	Microcrystalline matrix	0.71074	0.00002
PF33	17.80	Light-pink calcareous marl with root voids	8	Microcrystalline matrix	0.71069	0.00002
PF35	18.98	Light-pink calcareous marl with root voids	8	Microcrystalline matrix	0.71066	0.00001
PF38	21.10	Vari-coloured mud-supported conglomerate	6	Microcrystalline matrix	0.71067	0.00001
PF40	22.10	Red-brown mottled mudstone	7b	Microcrystalline carbonate streak	0.71061	0.00002
PF43	25.30	Red-brown mottled mudstone	7b	Microcrystalline matrix	0.71044	0.00002
PF46	28.37	Light-pink calcareous marl with root voids	8	Microcrystalline matrix	0.71046	0.00001
PF49	30.20	Light-pink calcareous marl with root voids	8	Microcrystalline matrix	0.71030	0.00002
PF54	33.10	Light-pink calcareous marl with root voids	8	Microcrystalline matrix	0.71037	0.00001
PF55	33.95	Yellow-brown fine-grained (calcareous) sandstone	4	Microcrystalline carbonate between sand grains	0.71045	0.00002
PF56	35.07	Red-brown mottled mudstone	7b	Microcrystalline carbonate streak	0.71033	0.00001
PF61	39.10	Red-brown mottled mudstone	7b	Microcrystalline matrix	0.71034	0.00002
PF63	41.80	Red-brown mottled mudstone	7b	Microcrystalline matrix	0.71030	0.00004
PF65	43.27	Red-brown mottled mudstone	7b	Microcrystalline matrix	0.71038	0.00002
PF67	45.35	Red-brown mottled mudstone	7b	Microcrystalline matrix	0.71036	0.00002

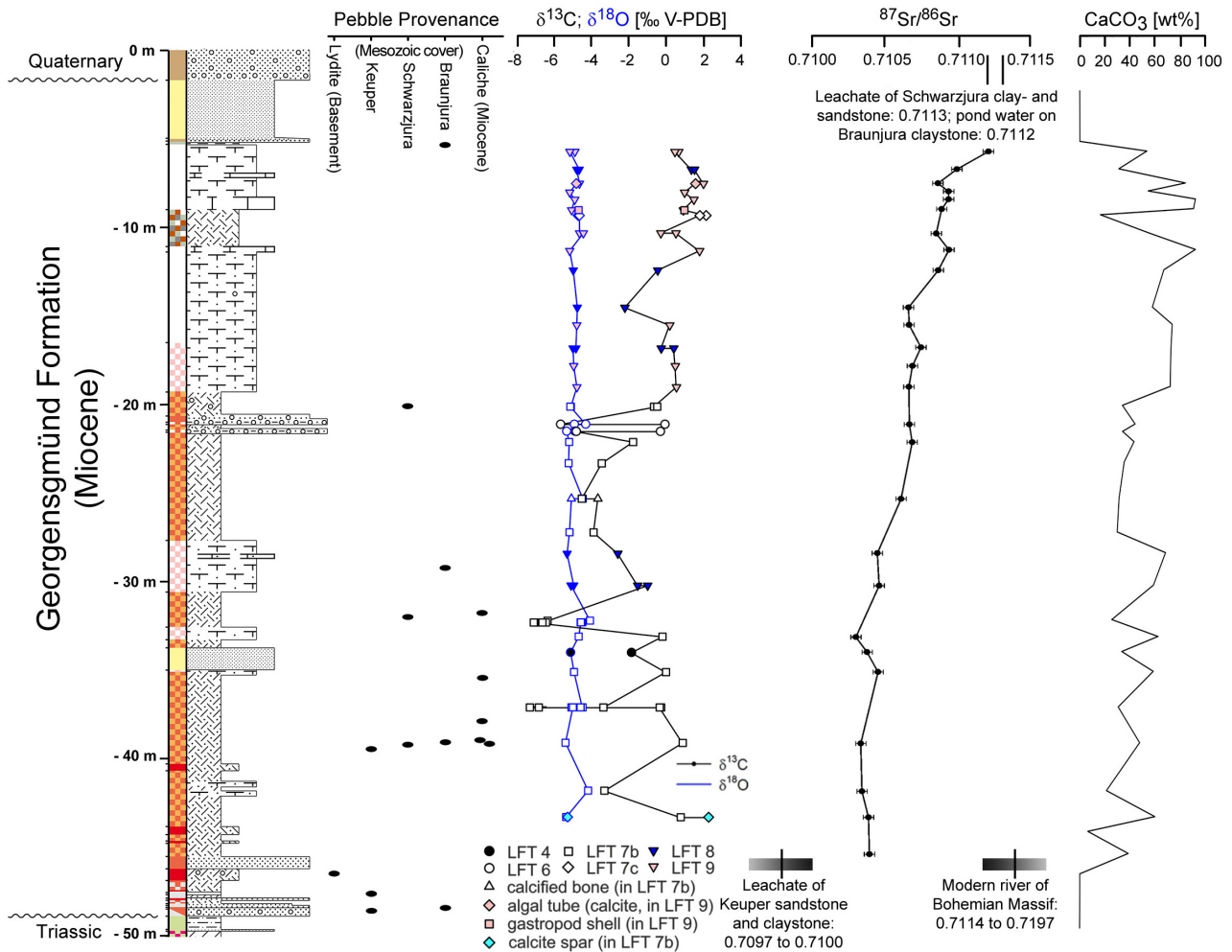


**Fig. 8.** Provenance of the pebbles, trend of  $\delta^{13}\text{C}$  and  $\delta^{18}\text{O}$  of the carbonates and  $^{87}\text{Sr}/^{86}\text{Sr}$  trend of the carbonates and carbonate contents in the investigated Pleinfeld drill section. The general trend of the increasing  $^{87}\text{Sr}/^{86}\text{Sr}$  trend is shown in comparison to  $^{87}\text{Sr}/^{86}\text{Sr}$  ratios of leachates from Schwarzhjura claystone and Keuper sandstone from Southern Germany (Ufrecht & Hölzl, 2006), pond water on Braunjura claystone of the Steinheim crater (Tütken *et al.*, 2006), and modern river water on Saxothuringian bedrock (Zieliński *et al.*, 2018).

well as fluvial settings (e.g. Newell *et al.*, 1999). The same applies to fine-grained sandstones (Cant, 1982; Fouch & Dean, 1982), palustrine limestones (Alonso-Zarza & Wright, 2010; Alonso-Zarza & Wright, 2010) and oncolitic tufa (e.g. Arenas *et al.*, 2007, 2010a, b).

In such cases, fossil assemblages are important criteria to distinguish between fluvial and lacustrine settings (Rust, 1982; Selley, 1992; Reading, 1996; Flügel, 2004). Indeed, the mollusc fauna of the Georgensmünd Formation is dominated by terrestrial taxa of pulmonate gastropods, and only a few aquatic representatives of Lymneidae and Planorbidae occur (Berger, 2010, 2013b). This fact was already noticed by Dorn (1939)

who, nonetheless, argued for a lacustrine setting. A further aquatic gastropod, the prosobranch *Hydrobia trochulus*, was mentioned by Gümbel (1891), Krumbeck (1926) and Dorn (1939) from the Bühl and Pleinfeld locations. This species is common in saline aquatic settings such as the Ries crater lake (e.g. Bolten, 1977). However, a re-investigation assigns these poorly preserved moulds to the freshwater hydrobiid genus *Heleobia* (Berger, 2013b; see also Kadolsky, 2008). The presence of the salinity-indicating taxon *Hydrobia trochulus*, as known from the saline Ries crater lake, therefore appears questionable. In any case, hydrobiid gastropods are not abundant or characteristic components of the



Georgensgmünd Formation. Consistent with these previous findings, the Pleinfeld drill core only yielded pulmonate gastropod fossils, specifically in LFTs 6, 8 and 9. There is no indication of aquatic gastropods. Likewise, other unequivocal aquatic organisms such as ostracods or bivalves are absent. The only exceptions are charophyte stem fragments in LFT 9b (Fig. 5E), which is a rare lithofacies type which, to date, is only known from the Bühl locality. While many charophytes occur in lakes as well as sluggish parts of rivers, the association of their fossil remains within a mud-supported fabric indicates deposition of LFT 9b in a standing water environment (floodplain pond or dammed area upstream of tufa barrages; e.g. Vázquez-Urbez *et al.*, 2012).

Indeed, sedimentological observations only provide a lack of evidence for a lacustrine origin of the formation. While clear bedding or lamination – characteristic of deposits in stagnant water bodies – is absent, the majority of the Pleinfeld deposits (for example, LFTs 7 to 9; Fig. 5A to F; Table 1) is poorly stratified or massive, with various features of pedogenesis. Only the vacuolar tufa LFT 10 may represent a spring deposit or small tufa barrage nearby a spring (see Manzo *et al.*, 2012; Perri *et al.*, 2012), and LFT 9b may represent a pond deposit, but both LFTs are rare and only observed at the Bühl locality.

However, further support for the fluvial interpretation comes from stable carbon and oxygen isotope ratios of the carbonate fraction of the samples. The data show a very distinct pattern, with strongly varying  $\delta^{13}\text{C}$  at almost constant  $\delta^{18}\text{O}$  values (Fig. 7A). This pattern is known from fluvial settings (for example, freshwater fluvial tufa deposits of the same region; Arp *et al.*, 2001) as well as from palaeosols (for example, Palaeogene Bighorn Basin; Koch *et al.*, 1995).

There is no covariation of  $\delta^{13}\text{C}$  and  $\delta^{18}\text{O}$  of the carbonate fraction along the entire profile (Fig. 7A,  $r = 0.44$ ,  $P < 0.05$ ,  $n = 55$ ) except for a weak covariation trend in the floodplain–palaeosol section ( $r = 0.77$ ,  $P < 0.05$ ,  $n = 22$ ). This isotopic pattern neither fits to hydrologically closed lakes showing a clear covariation (e.g. Talbot, 1990; Li & Ku, 1997; Utrilla *et al.*, 1998; Arp *et al.*, 2017a,b), nor to hydrologically open lakes, which are characterized by cloud-like  $\delta^{13}\text{C}$ – $\delta^{18}\text{O}$  patterns (e.g. Last *et al.*, 1994; Utrilla *et al.*, 1998; Hammarlund *et al.*, 2003; Benavente *et al.*, 2019) (Fig. 7B).

The narrow range of  $\delta^{18}\text{O}$  ( $-4.94 \pm 0.31\%$ ;  $n = 55$ ) in the Georgensgmünd Formation therefore indicates a short residence time of water, consistent with a fluvial setting. The only example of hydrologically open lake deposits with a similar stable isotope pattern is reported from the Eocene Fenghuoshan Group (Hoh-Xil Basin), with thin palustrine and shallow lacustrine limestone beds intercalated in a series of fluvial sandstones and red–brown floodplain mudstones (Cyr, 2004; Cyr *et al.*, 2005). These deposits are reminiscent of the Georgensgmünd lithofacies association; however, with a greater thickness and lateral extension. This example may underline that a low residence time of water (as derived from invariant  $\delta^{18}\text{O}$  values) is not definitive proof on its own for a fluvial setting. However, lipid biomarker analyses indicate that the Fenghuoshan Group carbonates suffered significant thermal alteration and the measured oxygen isotope values may not reflect primary values (Polissar *et al.*, 2009; Staisch *et al.*, 2014).

### Fluvial sub-environments and causes of lithofacies stacking patterns

A straightforward assignment of LFTs to specific fluvial sub-environments of this succession is hampered by the unknown geometry of beds. This is especially true for the coarse-grained siliclastic LFTs. Nonetheless, sedimentary structures, thickness information and stacking pattern allow a number of statements to be made.

**1 Fluvial floodplain.** Major parts of the Georgensgmünd Formation are composed of massive, mottled mudstone (LFT 7a, b and c). They are characterized by pedogenic features such as root voids, cutans, pedogenic slickensides, nodules and *in situ* brecciated microfabrics. Light to intense red–brown mottling indicates a successive change from a deeper soil zone with increasing groundwater saturation to prolonged oxygenation and palaeosol formation (Bown & Kraus, 1987; Alonso-Zarza, 2003). A weak covariation of  $\delta^{13}\text{C}$  and  $\delta^{18}\text{O}$  in carbonates from 22.10 to 43.27 m depth (LFTs 4, 7b and 8; PF38 to PF65,  $r = 0.71$ ;  $P < 0.05$ ) possibly indicates a minor evaporation effect on the floodplain (Bowen & Bloch, 2002; Leng & Marshall, 2004; Arenas *et al.*, 2010a, b).

**2 Palustrine swamp.** Carbonate-rich parts (LFT 8 and LFT 9a, b and c) of the core section show more characteristics of a water-saturated

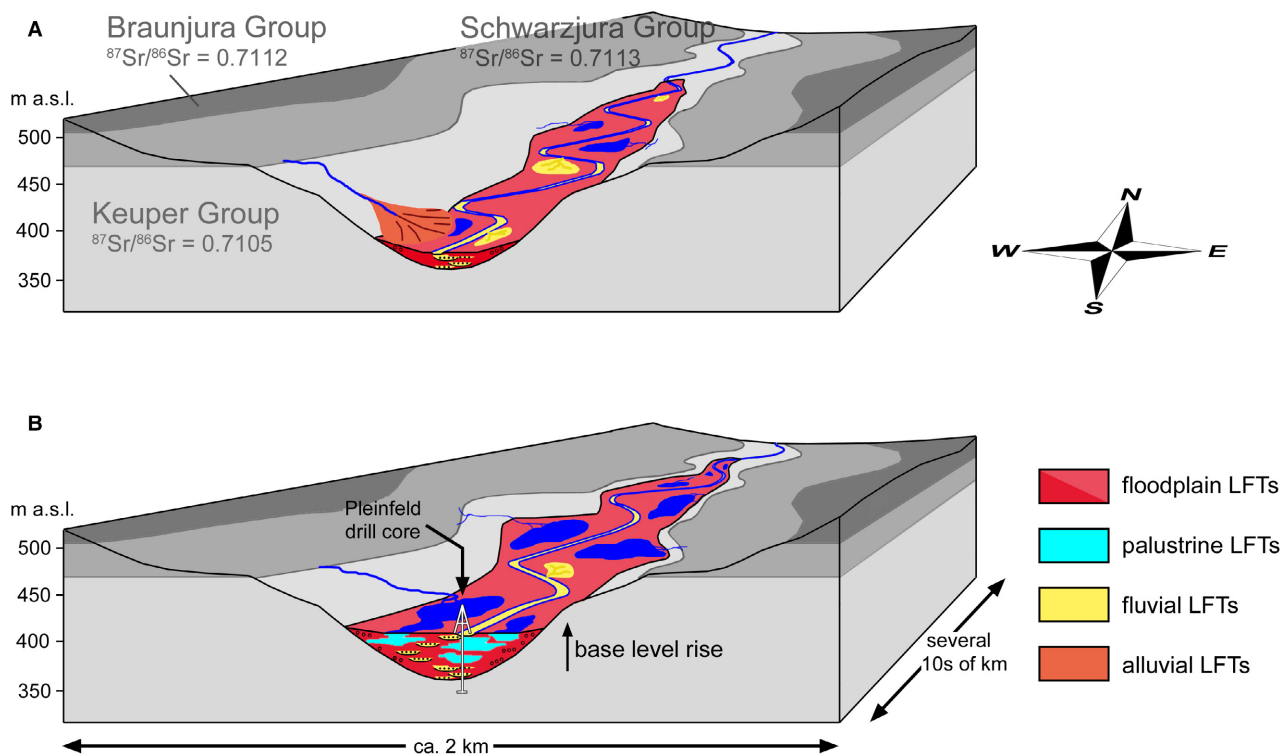


**Fig. 9.** Sedimentary model of (A) lower and (B) upper Georgensgmünd Formation. See Figs 1 and 2 for legends. During the early development of the formation (A), base-level was low and Triassic bedrocks are widely exposed in the Pleinfeld area. With the increasing base-level during the later development (B) Georgensgmünd Formation, Triassic Keuper bedrock was successively covered and the proportion of influx from the carbonate-bearing Schwarzzjura/Braunjura rocks increased. Weathering of Schwarzzjura/Braunjura rocks derived calcium-rich solutes to the depositional area, promoted the formation of calcareous palustrine deposit.  $^{87}\text{Sr}/^{86}\text{Sr}$  data represent leachates from Keuper and Schwarzzjura Group rocks, and pond water on Braunjura Group rocks.

and vegetated environment, when compared to the palaeosols described in the fluvial floodplain. Instead of intense red–brown mottling, the palustrine lithofacies shows a predominantly light pink to white–grey colour. Pulmonate gastropod shell debris and intense rooting of the mud-supported fabric suggest a swamp environment. Stratified, greenish clay-rich intercalations within LFT 8 (and charophytes in LFT 9b at the Bühl locality) are the only features that may point to temporary ponding.

**3 Debrisites.** Thin intercalations of mud-supported conglomerates (LFTs 5 and 6), with reworked components of the floodplain deposits and/or Mesozoic clasts, are interpreted as event deposits, reflecting heavy flooding. While a localized reworking within the floodplain sufficiently explains LFT 5, extraclasts embedded in a Jurassic-clay-derived matrix of LFT 6 point to a sediment gravity flow from the valley slope.

**4 Fluvial sands.** LFTs 1 to 4 are most difficult to interpret. Although bed thickness and sedimentary structures give some indication, no definitive distinction between channel, point bar, crevasse channel or crevasse splay deposits can be made from the drill core. Presumably, thin intercalations rather represent crevasse splay deposits, especially when affected by pedogenic concretionary carbonate (for example, LFT 4 at 33.75 to 35.00 m core depth). In turn, thicker and coarse-grained sandstones could be channel, point bar or crevasse channel deposits.

The cyclic stacking pattern and dominance of fine-grained floodplain and palustrine lithofacies, however, further constrains the depositional setting. Six cycles have been identified (Fig. 3). A complete cycle starts with coarse-grained to fine-grained sandstones (LFTs 1 to 4), followed by floodplain fines, which were

subjected to different extents of pedogenesis (LFT 7), and finally carbonate-rich palustrine swamp deposits (LFTs 8 and 9; Fig. 3). Non-cyclically intercalated mud conglomerates LFT 5 and LFT 6, in turn, reflect episodic flooding events.

Such fining-upward cycles are well-known from various river systems (for example, Alpine molasse deposits, Miall, 1996; Lower Old Red Sandstone of South Wales, Allen, 1965; Norian Arnstadt Formation, Beutler *et al.*, 1999; Arp *et al.*, 2005; Shukla *et al.*, 2006) and reflect auto-cyclic migration of a sinuous stream bed. However, typical features of braided river deposits such as amalgamating channel sandstones are absent in the investigated succession. Instead, the Georgensgmünd Formation is dominated by fine-grained floodplain deposits. Indeed, the gradient reconstruction of the ancient Moenodanuvius river by Hofbauer (2012) and Schirmer (2014) suggests a 50 m descent along the 40 km long river section at Pleinfeld, plausibly indicating a low-gradient river system (Schumm, 1985; Buffington & Montgomery, 2013). No climatic fluctuations can be derived from the cyclic lithofacies stacking pattern alone.

### Provenance of pebbles

The characteristic lithology of pebbles allows the identification of different older formations in the catchment of the Georgensgmünd Formation. Several groups of pebbles, derived from different formations, are identified (see section on *Pebble lithofacies*):

**1** The first group of clasts is considered to be derived from the Upper Triassic Keuper Group because of their lithological similarity (angular quartz grains, kaolinized feldspar) with the Keuper arkose in the lowermost part of the drill core.

**2** Similar to group (1), pebbles from group (2) are lithologically identical to rocks of the Sinemurian Gryphaeensandstein Formation ('Arietensandstein', Lower Jurassic Schwarzjura-Group; Berger *et al.*, 1971) of the region.

**3** Pebbles of group (3) superficially resemble Upper Jurassic limestone clasts. However, a thin section of the pebble at 32.30 m, containing pisoid fragments with coarsely laminated crusts within a clotted and rooted matrix (Fig. 6C) indicates a caliche origin. Another white-grey limestone pebble from 37.08 m depth also turned out to be of pedogenic origin.

**4** Group (4) pebbles are derived from siderite concretions, which are abundant in the Lower Jurassic Amaltheenton Formation and Middle Jurassic Opalinuston Formation of the region (Berger *et al.*, 1971). A limonite pebble at 48.60 m depth is possibly derived from the Middle Jurassic Eisensandstein Formation (Braunjura Group), while a 3.5 cm sized brown limonitic sandstone fragment with a bivalve mould at 5.15 m depth is clearly derived from this formation. Two 5 mm sized limonite pisoids ('pisolitic iron-ore'; Birzer, 1939) at -39.60 m depth indicate that components of Palaeogene-Neogene origin are present, too.

**5** For the last pebble group (5), i.e. the lydites, an origin from the Palaeozoic of the Frankenswald (north-western part of Saxothuringian in Fig. 1) is evident, i.e. 120 km NNE of the working area (Berger, 2013a).

Except for the lydite, all pebbles of the investigated drill core section can be derived from formations close to the Pleinfeld drill site. Specifically, clasts from the Upper Triassic Keuper Group, Lower Jurassic Schwarzjura and Middle Jurassic Braunjura Group are present and indicate sediment influxes from these formations and groups to the Georgensgmünd Formation. Upper Jurassic Weißjura limestone clasts, however, remain without evidence. All white-grey limestone pebbles turned out to be of pedogenic origin and appear to be reworked from lower Miocene caliche deposits. Indeed, Berger (2010) already questioned an Upper Jurassic Weißjura origin of similar clasts found at the Bühl locality.

The lydite pebble is the only evidence of long-distance transport, i.e. a provenance of isolated components in the Saxothuringian, 120 km NNE of the study area (Krumbeck, 1927; Dorn, 1939). However, most of the lydites of the Georgensgmünd Formation appear to be reworked from older, pre-Karpatian gravel deposits ('high-lying gravel', Dorn, 1939; Berger & Wittmann, 1968; Berger *et al.*, 1971; Berger, 2010), and their initial transport possibly dates back to the Early Cenozoic and Late Cretaceous (Lemcke, 1985; Berger, 2010: pp. 161–163, 165; Schirmer, 2014).

An important result is that no pebbles that were possibly reworked from ejecta of the Ries impact (i.e. Variscan crystalline rocks) or Mesozoic sedimentary rocks with internal fracturing or shock features, were found. The possibility of an effect of impact ejecta on the Moenodanuvius

drainage system, therefore, remains without evidence; this is consistent with the suggested pre-impact age (MN 5).

### Systematic change in sediment and water provenance in the catchment

Strikingly, the Mesozoic-derived pebbles of the drill core section show a clear trend from Keuper-derived pebbles (with few Jurassic pebbles) at the base to only Schwarzzura-derived and finally Braunjura-derived pebbles near the top of the section. Since both Keuper and Braunjura pebbles occur already at the base of the section, this trend cannot be explained by simple headward catchment erosion. Furthermore, the stratigraphic trend in clast provenance matches the successive, unidirectional increasing trend in  $^{87}\text{Sr}/^{86}\text{Sr}$  ratios (0.7103 to 0.7112) of the carbonates (Fig. 8). This trend is independent from  $\delta^{18}\text{O}$  values, suggesting that changes in water provenance occurred (e.g. Doebbert *et al.*, 2014).

With respect to the potential catchment area of the Georgensmünd Formation/Moenodanuvius, a number of  $^{87}\text{Sr}/^{86}\text{Sr}$  values from whole rock leachates are available for Triassic to Lower Jurassic formations (Ufrecht & Hölzl, 2006): Pure water leachates of Upper Triassic Keuper sandstones, arkoses and claystones show  $^{87}\text{Sr}/^{86}\text{Sr}$  values ranging from 0.7086 to 0.7140, with an average of 0.7105. On the other hand,  $^{87}\text{Sr}/^{86}\text{Sr}$  values of pure water leachates from Lower Jurassic claystones and sandstones reveal higher ratios, from 0.7102 to 0.7124, with an average  $^{87}\text{Sr}/^{86}\text{Sr}$  of 0.7113. A pond water sample on the Middle Jurassic Opalinuston revealed a  $^{87}\text{Sr}/^{86}\text{Sr}$  ratio of 0.7112 (Tütken *et al.*, 2006).

This increase in  $^{87}\text{Sr}/^{86}\text{Sr}$  of solutions probably reflects the fact that Keuper siliciclastics were largely derived from Variscan rocks (320 Ma) of the Bohemian Massif (i.e. the Saxothuringian and Moldanubian in Fig. 1), while Lower and Middle Jurassic siliciclastics have a mixed source and are derived from Variscan and older basement rocks ('Caledonian' and 'Cadomian'; 350 Ma and 580 Ma, respectively) from farther north-east and east (Paul *et al.*, 2008, 2009). Because  $^{87}\text{Sr}$  is generated by radiogenic decay of  $^{87}\text{Rb}$ , older rocks tend to have a higher  $^{87}\text{Sr}/^{86}\text{Sr}$  ratio (Faure & Powell, 1972). This explains the relatively low  $^{87}\text{Sr}/^{86}\text{Sr}$  values for Keuper siliciclastics and high  $^{87}\text{Sr}/^{86}\text{Sr}$  values for Jurassic siliciclastics, as the latter contain mica or other Rb-rich detrital minerals older in age. Finally,

Upper Jurassic groundwater shows much lower values (0.7075 to 0.7078), similar to the marine  $^{87}\text{Sr}/^{86}\text{Sr}$  signal for this time interval (Tütken *et al.*, 2006).

The unidirectional trend in  $^{87}\text{Sr}/^{86}\text{Sr}$  ratios in carbonates of the Pleinfeld section, therefore, perfectly mirrors the trend from Keuper-derived solutes to Schwarzzura-derived solutes and finally Braunjura-derived solutes (Fig. 8). Initial  $^{87}\text{Sr}/^{86}\text{Sr}$  values (0.7104) are close to the average Keuper leachate ratio (0.7105) and successively increase to  $^{87}\text{Sr}/^{86}\text{Sr}$  values identical to the Opalinuston pond water ratio (0.7112). Strikingly, this trend matches the trend in pebble provenance. In turn, there is no indication of a former influx of solutes from the Upper Jurassic Weißjura to the Georgensmünd Formation deposits at Pleinfeld. Indeed, a significant contribution of karstic waters from these marine carbonates should have led to much lower values and a decreasing trend in  $^{87}\text{Sr}/^{86}\text{Sr}$ , towards Upper Jurassic marine ratios (0.7068 to 0.7070; Veizer, 1989; Veizer *et al.*, 1999; Wierzbowski *et al.*, 2017).

A possible contribution of Variscan basement derived headwaters from the Frankenwald (i.e. the north-eastern part of the Saxothuringian in Fig. 1), however, is more difficult to demonstrate on basis of the current data. Anthropogenically uncontaminated headwaters of modern rivers draining Saxothuringian bedrocks of the northern Bohemian Massif show  $^{87}\text{Sr}/^{86}\text{Sr}$  ratios ranging from 0.7114 to 0.7197 at low Sr concentrations of 64 to 117 ppb [Zieliński *et al.*, 2018 (sites N14, K2, Br4, Br5 and B3)]. Solutes carrying this high  $^{87}\text{Sr}/^{86}\text{Sr}$  signal may have contributed to the riverine waters of the working area, but dilution along the >120 km long Moenodanuvius river certainly obliterated any significant impact on the  $^{87}\text{Sr}/^{86}\text{Sr}$  in the carbonates of the Pleinfeld drill core.

### Major control of fluvial sedimentation: climate change versus base-level change

Continental sedimentary successions are sensitive to climatic changes as well as to base-level changes governed by upstream controls (for example, tectonic movements) and/or downstream controls (for example, sea-level or lake level change) (Carroll & Bohacs, 1999; Bohacs *et al.*, 2000; Cohen, 2003; Arenas *et al.*, 2010a; Tanner, 2010). Many of these continental sedimentary successions comprise red-brown siliciclastics ('red beds'; e.g. van Houten, 1973).

Likewise, carbonate contents in terrestrial successions have been taken as a palaeoclimate proxy reflecting humid or arid condition (e.g. Chen *et al.*, 1999; Yan *et al.*, 2017).

Among these deposits, red–brown mottled mudstones are common floodplain sediments that reflect good drainage and temporary, well-oxidized conditions (Sheldon, 2005). They commonly, though not necessarily (Sheldon, 2005; Song *et al.*, 2018), reflect semi-arid or even arid climatic conditions (Kraus, 1987; Kraus & Aslan, 1993; Mack & James, 1994). Carbonate precipitates within these mottled mudstones reflect capillary rise of groundwater at times of reduced siliciclastic influx (Semeniuk & Meagher, 1981; Wright *et al.*, 1988; Tandon & Gibling, 1994).

Palustrine limestones and marlstones, on the other hand, essentially form under semi-arid to sub-humid conditions (Platt & Wright, 1992; Alonso-Zarza, 2003; Alonso-Zarza *et al.*, 2012), with more arid phases recognizable by extensive calcretization (Djamali *et al.*, 2006) or dolomite (Abdul Aziz *et al.*, 2000). Wetter conditions are indicated by extensive rooting, specific pulmonate gastropods and the absence of evaporites (Platt & Wright, 1992). Moreover, comparatively low  $\delta^{18}\text{O}$  values in palustrine limestones have been taken as an argument for wetter conditions, if compared to contemporaneous palaeosol carbonates (Bowen & Bloch, 2002).

At first glance, the observed lithofacies change within the investigated Georgensgmünd Formation (Fig. 3) may therefore reflect a climatic change. The lower part of the section is dominated by red–brown carbonate-poor mottled mudstones, which may point to conditions that are more arid. In turn, parts with light-coloured palustrine limestones, which contain abundant root voids and pulmonate gastropods, could reflect a change to more humid conditions.

However, the carbonate stable oxygen isotopes of the investigated succession show a strikingly low variance at  $\delta^{18}\text{O} = -4.94 \pm 0.31\text{‰}$  ( $n = 55$ ), across all lithofacies types analyzed (Figs 7 and 8). No systematic  $\delta^{18}\text{O}$  trend is observed along the section, suggesting a hydrologically stable condition. Neither significant changes in evaporation, inflow–outflow ratio, ambient temperatures, nor changes in the continental effect during the deposition of the Georgensgmünd Formation are evident.

Likewise, no general trend in carbonate  $\delta^{13}\text{C}$  is observed along the section, although (in contrast to  $\delta^{18}\text{O}$ )  $\delta^{13}\text{C}$  values vary considerably (Fig. 7A). Specifically,  $\delta^{13}\text{C}$  variations coincide

with changes in lithofacies, with low values in floodplain palaeosol nodules (LFTs 6 and 7:  $\delta^{13}\text{C} = -2.57 \pm 2.63\text{‰}$ ;  $n = 22$ ) and reworked caliche pebbles (within LFT 7:  $\delta^{13}\text{C} = -6.93 \pm 0.30\text{‰}$ ;  $n = 5$ ), and high values in floodplain pond and spring-fed carbonates (LFTs 9b, 9c and 10:  $\delta^{13}\text{C} = 3.04 \pm 2.44\text{‰}$ ;  $n = 7$ ).

The latter high values probably reflect a photosynthesis effect by cyanobacteria or eukaryotic algae within the shallow ponds and a  $\text{CO}_2$  degassing effect at spring sites (LFTs 9b, 9c and 10), where discharging waters initially show intermediate  $\delta^{13}\text{C}_{\text{DIC}}$  values reflecting a mixture of dissolved inorganic carbon (DIC) from Jurassic carbonate (Fig. 7B) and soil-derived  $\text{CO}_2$ . Nonetheless,  $\delta^{13}\text{C}$  values in LFT 9 and LFT 10 are higher than similar present-day and Quaternary tufa and pond deposits (e.g. Andrews *et al.*, 1997; Mayer & Schwark, 1999; Arp *et al.*, 2001; Valero Garcés *et al.*, 2008; Arenas *et al.*, 2010a, 2019; Fig. 7B). While temporary anaerobic conditions may have occurred in floodplain pond sediments (and palustrine sediments), the lack of extremely high  $\delta^{13}\text{C}$  values (see Talbot & Kelts, 1986) indicates that methanogenesis and associated  $\text{CH}_4$  loss did not affect the DIC pool significantly. Likewise, the invariant  $\delta^{18}\text{O}$  argues against an evaporation effect, which should have affected both  $\delta^{13}\text{C}$  and  $\delta^{18}\text{O}$  simultaneously. Instead, climatic conditions warmer than present-day (Methner *et al.*, 2020) may have enhanced aquatic productivity, thereby causing a higher  $^{12}\text{C}$  depletion of surface waters in this region if compared to today.

In turn, the former, low values, are characteristic of  $^{13}\text{C}$ -depleted  $\text{CO}_2$  from respiratory processes in soils (LFTs 6 and 7) (e.g. Stevenson, 1969; Kraus, 1987; Quade *et al.*, 1989; Whittar, 1999). Values of palustrine facies types (LFTs 8 and 9a) vary between these end members (Fig. 7A). A potential, increasing admixture of DIC from marine Jurassic carbonate to the top of the section (Fig. 8) appears possible, but remains unresolvable against the background of strong  $\delta^{13}\text{C}$  variations within the pedogenesis-affected lithofacies types (for example, at 37.1 m depth; Fig. 8). Likewise, there is no indication of potential post-Miocene meteoric diagenetic alterations of microcrystalline carbonate  $\delta^{13}\text{C}$  values in top parts of the section. None of these samples shows a decrease in  $\delta^{13}\text{C}$  associated with a shift of  $\delta^{18}\text{O}$  towards meteoric values as it is seen in a late diagenetic spar cement (Fig. 7A) or present-day tufa carbonate of the region (Fig. 7B).



No climatic trend related to possible atmospheric  $p\text{CO}_2$  changes can be derived on the basis of these data. This would be consistent with a pre-impact age of the Georgensgmünd Formation, falling in the time range of the Miocene Climatic Optimum (MCO; e.g. Zachos *et al.*, 2001), as opposed to the post-impact scenario and time of the mid-Miocene Climate Transition (MMCT; e.g. Methner *et al.*, 2020).

On the other hand, a clear change in the provenance of water and sediment is evident from the change in pebble lithology and  $^{87}\text{Sr}/^{86}\text{Sr}$  values of carbonates (Fig. 8). Both signatures suggest a change from water and sediment predominantly derived from the Keuper Group to the Schwarzhura and Braunjura groups. This trend of changing provenance can be explained by a rise in base-level (Holbrook *et al.*, 2006; Catuneanu *et al.*, 2009), either by downstream controls (for example, sea level rise) and/or upstream controls (for example, regional subsidence or increasing rainfall). Likewise, a rise in base-level controlled by upstream factors explains, without any change in climate, the trend of increasing carbonate contents from the base to the top of the Georgensgmünd Formation: Initial waters derived from the Keuper Group are poor in carbonate (Fig. 9A), while their later replacement by waters from Lower/Middle Jurassic calcareous claystones and marlstones supplied sufficient calcium and carbonate to enhance the formation of palustrine lime-stones (Fig. 9B).

Indeed, base-level changes are known from a number of studies as a major steering factor for fluvial and floodplain successions and their palaeosol development (e.g. Leeder, 1975; Schumm, 1993; Leeder & Stewart, 1996; Pla-Pueyo *et al.*, 2009). Specifically, base-level changes may alter fluvial style (slope and gradient, sinuosity, channel parameters), sediment supply, accommodation spaces and groundwater table (Wright & Marriott, 1993; Miall, 1996; Ethridge *et al.*, 1999; Blum & Törnqvist, 2000; Alonso-Zarza, 2003; Pla-Pueyo *et al.*, 2009). Furthermore, the adjacent Northern Alpine Foreland Basin (NAFB), in which the Moenodanuvius drained, experienced several marine incursions and regressions (see Fig. 2; Reuter, 1927; Lemcke, 1975; Doppler & Schwerd, 1996), which are considered as eustatic sea-level changes (Bachmann *et al.*, 1987; Bachmann & Müller, 1992; Jin *et al.*, 1995; Zweigel *et al.*, 1998).

A detailed comparison with the third-order sequences of the central Paratethys (Piller

*et al.*, 2007), the marine incursions and regressions in the NAFB (western Paratethys; Pippèr & Reichenbacher, 2017, and references therein), however, suggests that the Georgensgmünd Formation accumulated simultaneously with sea-level fall and lowstand conditions (Fig. 2). Indeed, early Upper Freshwater Molasse deposits (Fig. 2) of the NAFB also progressively overstep the karstic plateau of the southern Franconian and Swabian Alb (pre-Ries-impact 'limnic lower series'; Doppler *et al.*, 2002) at the same time, forming a low-relief swampy landscape (Doppler *et al.*, 2002) with local caliche development (Bolten & Müller, 1969).

This means that the base-level rise controlled sedimentation of the Georgensgmünd Formation (Fig. 9) is caused by a tectonic subsidence in this region (Bolten & Müller, 1969: p. 121; Doppler *et al.*, 2002), independent from sea-level changes. Later tectonic movement, leading to uplift and minor tilting of the whole region is indicated by tilting of the lower Miocene cliff line [Fig. 2; 'post-middle Miocene tilting' (Gall, 1974); 'during the Pliocene' (Doppler *et al.*, 2002)].

## CONCLUSIONS

**1** Despite the fact that the impact ejecta covers the downstream fluvial section, no traces of damming and possible lake evolution are seen, because only pre-impact fluvial deposits are preserved. Instead, lithofacies associations (dominance of fine-grained lithofacies types), sedimentary structures (lack of lamination), fossils (lack of lacustrine organisms), and stable oxygen and carbon isotopes (strong variation in  $\delta^{13}\text{C}$  at almost constant  $\delta^{18}\text{O}$ ) point to a low-gradient river system with a narrow stream bed and dominant floodplains. This interpretation is consistent with a pre-Ries-impact age of the formation suggested by Berger (2010), implying that its sedimentation is unrelated to impact ejecta damming.

**2** The observed trend in sediment lithofacies within the formation, from red-brown carbonate-poor siliciclastics to white-grey palustrine limestones, is unrelated to climatic changes. Constant carbonate oxygen isotope ratios throughout the section point to constant climatic conditions.

**3** Instead, a unidirectional increase in  $^{87}\text{Sr}/^{86}\text{Sr}$  in carbonates and a change of pebble

provenance from Keuper to Schwarz and Braunjura parent rocks indicate that a base-level rise in this region controlled fluvial sedimentation and lithofacies succession. A comparison with sea-level changes in the adjacent Northern Alpine Foreland Basin suggests that this base-level rise is tectonically induced.

4 In drill core sections, where the three-dimensional geometry of beds is unknown, the distinction of lacustrine and fluvial deposits can be made using palaeontological and lithofacies criteria (presence or absence of lacustrine organisms and laminated mudstones) in combination with carbonate stable isotope signatures (invariant  $\delta^{18}\text{O}$  at highly variable  $\delta^{13}\text{C}$ ). The provenance of extraclasts and changes in carbonate  $^{87}\text{Sr}/^{86}\text{Sr}$  ratios allow the differentiation of climatic and regional geological effects, such as changes in catchment area and base-level.

## ACKNOWLEDGEMENTS

We thank Birgit Röring, Wolfgang Dröse and Axel Hackmann for lab. support. We are also grateful to Dennis Kohl and Andreas Pack for stable isotope analysis. We are indebted to James W. Head for his suggestions in an earlier version of the manuscript. Three anonymous reviewers, Associate Editor Concha Arenas and Chief Editor Giovanna Della Porta provided valuable suggestions to improve the manuscript. The study was supported by the German Research Foundation (project AR 335/9-1), the China Scholarship Council 201708510097 (CSC scholarship to LZ), and the "Freunde des Rieskratermuseums". Funding Statement: Open Access funding enabled and organized by Projekt DEAL. WOA Institution: GEORG-AUGUST-UNIVERSITÄT GÖTTINGEN. Blended DEAL: Projekt DEAL.

## DATA AVAILABILITY STATEMENT

The data that support the findings of this study are available in the manuscript or in the supplementary material.

## REFERENCES

- Abdul Aziz, H., Hilgen, F., Krijgsman, W., Sanz, E. and Calvo, J. (2000) Astronomical forcing of sedimentary cycles in the middle to late Miocene continental Calatayud Basin (NE Spain). *Earth Planet. Sci. Lett.*, **177**, 9–22.
- Agustí, J., Cabrera, L., Garcés, M., Krijgsman, W., Oms, O. and Parés, J.M. (2001) A calibrated mammal scale for the Neogene of Western Europe. State of the art. *Earth-Sci. Rev.*, **52**, 247–260.
- Allen, J.R.L. (1965) Fining-upwards cycles in alluvial successions. *Geol. J.*, **4**, 229–246.
- Allen, J.P., Fielding, C.R., Gibling, M.R. and Rygel, M.C. (2014) Recognizing products of palaeoclimate fluctuation in the fluvial stratigraphic record: An example from the Pennsylvanian to Lower Permian of Cape Breton Island, Nova Scotia. *Sedimentology*, **61**, 1332–1381.
- Alonso-Zarza, A.M. (2003) Palaeoenvironmental significance of palustrine carbonates and calcretes in the geological record. *Earth-Sci. Rev.*, **60**, 261–298.
- Alonso-Zarza, A.M., Meléndez, A., Martín-García, R., Herrero, M.J. and Martín-Pérez, A. (2012) Discriminating between tectonism and climate signatures in palustrine deposits: Lessons from the Miocene of the Teruel Graben, NE Spain. *Earth-Sci. Rev.*, **113**, 141–160.
- Alonso-Zarza, A.M. and Wright, V.P. (2010) Chapter 2: Palustrine Carbonates. In: *Developments in Sedimentology*, Vol. **61** (Eds Alonso-Zarza, A.M. and Tanner, L.H.), pp. 103–131. Elsevier, The Netherlands.
- Andrews, J. (2006) Palaeoclimatic records from stable isotopes in riverine tufas: synthesis and review. *Earth-Sci. Rev.*, **75**, 85–104.
- Andrews, J.E., Riding, R. and Dennis, P.F. (1997) The stable isotope record of environmental and climatic signals in modern terrestrial microbial carbonates from Europe. *Palaeogeogr. Palaeoclimatol. Palaeoecol.*, **129**, 171–189.
- Arenas, C., Cabrera, L. and Ramos, E. (2007) Sedimentology of tufa facies and continental microbialites from the Palaeogene of Mallorca Island (Spain). *Sed. Geol.*, **197**, 1–27.
- Arenas, C., Osácar, C., Sancho, C., Vázquez-Urbez, M., Auqué, L. and Pardo, G. (2010a) Seasonal record from recent fluvial tufa deposits (Monasterio de Piedra, NE Spain): sedimentological and stable isotope data. *Geol. Soc. London Spec. Publ.*, **336**, 119.
- Arenas, C., Osácar, M.C., Auqué, L. and Sancho, C. (2019) Coupling textural and stable-isotope variations in fluvial stromatolites: Comparison of Pleistocene and recent records in NE Spain. *J. Palaeogeogr.*, **8**, e13.
- Arenas, C., Vázquez-Urbez, M., Pardo-Tirapu, G. and Sancho-Marcén, C. (2010b) Fluvial and associated carbonate deposits. In: *Developments in Sedimentology*, Vol. **61** (Eds Alonso-Zarza, A.M. and Tanner, L.H.), pp. 133–175. Elsevier, The Netherlands.
- Arp, G., Bielert, F., Hoffmann, V.-E. and Löffler, T. (2005) Palaeoenvironmental significance of lacustrine stromatolites of the Arnstadt Formation ("Steinmergelkeuper", Upper Triassic, N-Germany). *Facies*, **51**, 419–441.
- Arp, G., Hansen, B.T., Pack, A., Reimer, A., Schmidt, B.C., Simon, K. and Jung, D. (2017a) The soda lake—mesosaline halite lake transition in the Ries impact crater basin (drilling Löpsingen 2012, Miocene, southern Germany). *Facies*, **63**, 1.
- Arp, G., Kolepka, C., Simon, K., Karius, V., Nolte, N. and Hansen, B.T. (2013) New evidence for persistent impact-generated hydrothermal activity in the Miocene Ries impact structure, Germany. *Meteorit. Planet. Sci.*, **48**, 2491–2516.
- Arp, G., Ulbrich, P., Reimer, A., Hartmann, G. and Jung, D. (2017b) Süßwassermügel der Kraterrandhöhen des

- Nördlinger Rieses (Miozän): Relikte einer Aussüßungsphase des Riesees? *Geologische Blätter für Nordost-Bayern*, **67**, 19–34.
- Arp, G., Wedemeyer, N. and Reitner, J. (2001) Fluvial tufa formation in a hard-water creek (Deinschwanger Bach, Franconian Alb, Germany). *Facies*, **44**, 1–22.
- Bachmann, G.H., Müller, M. and Weggen, K. (1987) Evolution of the Molasse Basin (Germany, Switzerland). *Tectonophysics*, **137**, 77–92.
- Bachmann, G. and Müller, M. (1992) Sedimentary and structural evolution of the German Molasse Basin. *Eclogae Geol. Helvet.*, **85**, 519–530.
- Bader, K., Meyer, R.K.F. and Brunold, H. (2000) Graupensandrinne-Urnaabrinne, ihre Verbindung und tektonische Verstellung zwischen Donauworth und Regensburg. *Geologica Bavarica*, **105**, 243–250.
- Bailey, T.R., McArthur, J.M., Prince, H. and Thirlwall, M.F. (2000) Dissolution methods for strontium isotope stratigraphy: whole rock analysis. *Chem. Geol.*, **167**, 313–319.
- Bellefroid, E.J., Planavsky, N.J., Miller, N.R., Brand, U. and Wang, C. (2018) Case studies on the utility of sequential carbonate leaching for radiogenic strontium isotope analysis. *Chem. Geol.*, **497**, 88–99.
- Benavente, C.A., Mancuso, A.C. and Bohacs, K.M. (2019) Paleohydrogeologic reconstruction of Triassic carbonate paleolakes from stable isotopes: Encompassing two lacustrine models. *J. S. Am. Earth Sci.*, **95**, 102292.
- Berger, G. (2010) Die miozäne Flora und Fauna (MN5) der historischen Fossil-Lagerstätte Georgensgmünd (Mfr.): unter Berücksichtigung der Ablagerungen des Urmaintals zwischen Roth und Treuchtlingen. *Abhandlungen der Naturhistorischen Gesellschaft Nürnberg*, **46**, 1–191.
- Berger, G. (2013a) Graptolithen aus Lyditgeröllen und untermiozäne Sedimente zwischen Schwabach und Roth. *Natur Mensch*, **2011**, 107–111.
- Berger, G. (2013b) Erstfunde von untermiozänen (MN 5) Säugetierüberresten bei Rittersbach (Mittelfranken). *Natur Mensch*, **2012**, 105–118.
- Berger, K. (1973) Obermiozäne Sedimente mit Süßwasserkalken im Rezat-Rednitz-Gebiet von Pleinfeld-Spalt und Georgensgmünd/Mfr. *Geologica Bavarica*, **67**, 238–248.
- Berger, K., Apel, R., Bader, K. and Diez, T. (1971) *Geologische Karte von Bayern 1:25000 Erläuterungen zum Blatt Nr. 6831 Spalt*. Bayerisches Geologisches Landesamt, München.
- Berger, K., Apel, R., Bader, K., Kröger, J., Schmidt-Kaler, H., Wellnhöfer, P. and Wittmann, O. (1982) *Geologische Karte von Bayern 1:25000 Erläuterungen zum Blatt Nr. 6931 Weißenburg i. Bay.* Bayerisches Geologisches Landesamt, Munich.
- Berger, K. and Wittmann, O. (1968) *Geologische Karte von Bayern 1:25000 Erläuterungen zum Blatt Nr. 6832 Heideck*. Bayerisches Geologisches Landesamt, Munich.
- Beutler, G., Hauschke, N. and Nitsch, E. (1999) Faziesentwicklung des Keupers im Germanischen Becken. In: *Trias-Eine ganz andere Welt*. (Ed. Wilde, V.), pp. 129–174. Pfeil Verlag, Munich.
- Birck, J.L. (1986) Precision K-Rb-Sr isotopic analysis: application to Rb-Sr chronology. *Chem. Geol.*, **56**, 73–83.
- Birzer, F. (1939) Verwitterung und Landschaftsgeschichte in der südlichen Frankenalb. *Zeitschrift der Deutschen Geologischen Gesellschaft*, **91**, 1–57.
- Birzer, F. (1969) Molasse und Ries-Schutt im westlichen Teil der südlichen Frankenalb. *Geologische Blätter für Nordost-Bayern*, **19**, 1–28.
- Blum, M.D. and Törnqvist, T.E. (2000) Fluvial responses to climate and sea-level change: a review and look forward. *Sedimentology*, **47**, 2–48.
- Bohacs, K.M., Carroll, A.R., Neal, J.E. and Mankiewicz, P.J. (2000) Lake-basin type, source potential, and hydrocarbon character: an integrated sequence-stratigraphic-geochemical framework. *AAPG Stud. Geol.*, **46**, 3–34.
- Bolten, R.H. (1977) *Die Karbonatischen Ablagerungen des obermiozänen Kratersees im Nördlinger Ries*. Ludwig-Maximilians-Universität, München, 288 + XXI pp.
- Bolten, R. and Müller, D. (1969) Das Tertiär im Nördlinger Ries und in seiner Umgebung. *Geologica Bavarica*, **61**, 87–130.
- Bowen, G.J. and Bloch, J.I. (2002) Petrography and geochemistry of floodplain limestones from the Clarks Fork Basin, Wyoming, USA: carbonate deposition and fossil accumulation on a Paleocene-Eocene floodplain. *J. Sed. Res.*, **72**, 46–58.
- Bown, T.M. and Kraus, M.J. (1987) Integration of channel and floodplain suites; I, Developmental sequence and lateral relations of alluvial Paleosols. *J. Sed. Res.*, **57**, 587–601.
- Buffington, J. and Montgomery, D. (2013) Geomorphic classification of rivers. In: *Treatise on Geomorphology, Fluvial Geomorphology*, vol. 9 (Eds Shroder, J. and Wohl, E.), pp. 730–767. Academic Press, San Diego, CA.
- Cant, D.J. (1982) Fluvial facies models and their application. In: *Sandstone Depositional Environments* (Eds Scholle, P.A. and Spearing, D.), *AAPG Memoir*, **31**, 115–137.
- Carroll, A.R. and Bohacs, K.M. (1999) Stratigraphic classification of ancient lakes: Balancing tectonic and climatic controls. *Geology*, **27**, 99–102.
- Catuneanu, O., Abreu, V., Bhattacharya, J., Blum, M., Dalrymple, R., Eriksson, P., Fielding, C.R., Fisher, W., Galloway, W. and Gibling, M. (2009) Towards the standardization of sequence stratigraphy. *Earth-Sci. Rev.*, **92**, 1–33.
- Chen, F.H., Bloemendal, J., Zhang, P.Z. and Liu, G.X. (1999) An 800 ky proxy record of climate from lake sediments of the Zoige Basin, eastern Tibetan Plateau. *Palaeogeogr. Palaeoclimatol. Palaeoecol.*, **151**, 307–320.
- Clemmensen, L.B., Kent, D.V. and Jenkins, F.A. (1998) A Late Triassic lake system in East Greenland: facies, depositional cycles and palaeoclimate. *Palaeogeogr. Palaeoclimatol. Palaeoecol.*, **140**, 135–159.
- Cohen, A.S. (2003) *Palaeolimnology: the history and evolution of lake systems*. Oxford University Press, New York, NY, 500 pp.
- Cyr, A.J. (2004) *Geochemical and Stable Isotopic Evaluation of Fenghuoshan Group Lacustrine Carbonates, North-Central Tibet: Implications for the Palealtimetry of the Mid-Tertiary Tibetan Plateau* (Thesis). Miami University, Miami, FL.
- Cyr, A.J., Currie, B.S. and Rowley, D.B. (2005) Geochemical Evaluation of Fenghuoshan Group Lacustrine Carbonates, North-Central Tibet: Implications for the Palealtimetry of the Eocene Tibetan Plateau. *J. Geol.*, **113**, 517–533.
- Demko, T.M., Currie, B.S. and Nicoll, K.A. (2004) Regional paleoclimatic and stratigraphic implications of paleosols and fluvial/overbank architecture in the Morrison Formation (Upper Jurassic), Western Interior, USA. *Sed. Geol.*, **167**, 115–135.
- Djamali, M., Soulié-Marsche, I., Esu, D., Gliozzi, E. and Okhravi, R. (2006) Palaeoenvironment of a Late Quaternary lacustrine-palustrine carbonate complex:

- Zarand Basin, Saveh, central Iran. *Palaeogeogr. Palaeoclimatol. Palaeoecol.*, **237**, 315–334.
- Doebbert, A.C., Johnson, C.M., Carroll, A.R., Beard, B.L., Pietras, J.T., Carson, M.R., Norsted, B. and Throckmorton, L.A.** (2014) Controls on Sr isotopic evolution in lacustrine systems: Eocene green river formation. *Wyoming. Chem. Geol.*, **380**, 172–189.
- Doppler, G., Fiebig, M. and Meyer, R.** (2002) *Erläuterungen zur Geologischen Karte 1: 100.000, Geowissenschaftliche Landesaufnahme in der Planungsregion 10 Ingolstadt*, pp. 1–179. Bayerisches Geologisches Landesamt, München.
- Doppler, G. and Schwerd, K.** (1996) Gesteinsfolge des Molassebeckens und der inneralpinen Tertiärbecken. Faltenmolasse, Aufgerichtete Molasse und westliche Vorlandmolasse. In: *Erläuterungen zur Geologischen Karte von Bayern 1:500000* (Eds Freudenberger, W. and Schwerd, K.), pp. 150–168. Bayerisches Geologisches Landesamt, München.
- Dorn, C.** (1939) Die Ablagerungen der obermiocänen Süßwasserkalke bei Pleinfeld und Georgsgemünd in Mittelfranken. *Jahresberichte und Mitteilungen des Oberheinhischen Geologischen Vereins, Neue Folge*, **28**, 67–98.
- Ekart, D.D., Cerling, T.E., Montanez, I.P. and Tabor, N.J.** (1999) A 400 million year carbon isotope record of pedogenic carbonate: implications for paleoatmospheric carbon dioxide. *Am. J. Sci.*, **299**, 805–827.
- Ethridge, F., Skelly, R. and Bristow, C.** (1999) Avulsion and crevasing in the sandy, braided Niobrara River: complex response to base-level rise and aggradation. In: *Fluvial Sedimentology VI* (Eds Smith, N.D. and Rogers, J.), *Int. Assoc. Sedimentol. Spec. Publ.*, **28**, 179–192.
- Faure, G.** (1986) In: *Principles of Isotope Geology*, 2nd edn. John Wiley & Sons, New York, NY, 589 pp.
- Faure, G. and Powell, J.** (1972) *Strontium isotope geology*. Springer-Verlag, Berlin, 189 pp.
- Fischer, K.** (1983) Die Reliefentwicklung im Osten des Rieses. In: *Verein Rieser Kulturtag (Hrsg.)*, **IV**, pp. 564–588. Rieser Kulturtag, Dokumentation, Nördlingen.
- Flügel, E.** (2004) *Microfacies of Carbonate Rocks: Analysis, Interpretation and Application*. Springer, Berlin, Heidelberg.
- Fouch, T. and Dean, W.** (1982) Lacustrine and associated clastic depositional environments. In: *Sandstone Depositional Environments* (Eds Scholle, P.A. and Spearing, D.), *AAPG Memoir*, **31**, 87–114.
- Freudenberger, W.** (1996) *Erläuterungen zur geologischen Karte von Bayern*. Bayerisches Geologisches Landesamt, München.
- Gall, H.** (1974) Neue Daten zum Verlauf der Klifflinie der Oberen Meeresmolasse (Helvet) im südlichen Vorries. *Mitt. Bayer. Staatssamml. Paläont. hist. Geologie*, **14**, 81–101.
- Gierlowski-Kordesch, E., Jacobson, A., Blum, J. and Valero Garcés, B.L.** (2008) Watershed reconstruction of a Paleocene-Eocene lake basin using Sr isotopes in carbonate rocks. *Geol. Soc. Am. Bull.*, **120**, 85–95.
- Gümbel, C.W.** (1891) *Geognostische Beschreibung der Fränkischen Alb (Frankenalb) mit dem anstossenden Fränkischen Keupergebiete: Geognostische Beschreibung des Königreichs Bayern, Abtheilung 4*. Fischer, Kassel, 763 pp.
- Hammarlund, D., Björck, S., Buchardt, B., Israelson, C. and Thomsen, C.T.** (2003) Rapid hydrological changes during the Holocene revealed by stable isotope records of lacustrine carbonates from Lake Igelsjön, southern Sweden. *Quatern. Sci. Rev.*, **22**, 353–370.
- Hardenbol, J., Thierry, J., Farley, M.B., Jacquin, T., Graciansky, P.C. and Vail, P.R.** (1998) Mesozoic and Cenozoic Sequence Chronostratigraphic Framework of European Basins. In: *Mesozoic and Cenozoic sequence stratigraphy of European basins*, vol. **60** (Eds Graciansky, C.-P., Hardenbol, J., Jacquin, T. and Vail, P.R.), *SEPM Spec. Publ.*, **60**, 3–13.
- Haunschild, H.** (1992) Die Thermalwasser-Erschließungsbohrung Treuchtlingen 2 (T 2)-Kurzmitteilung. *Geologische Blätter für NO-Bayern*, **42**, 269–276.
- Hofbauer, G.** (2001) Die Diskussion um die Entstehung der Süddeutschen Schichtstufenlandschaft: Eine historischmethodologische Skizze mit einem Modell zur fluvial gesteuerten Schichtstufen-Morphogenese. *Natur und Mensch, Jahresmitteilungen der Naturhistorischen Gesellschaft Nürnberg eV, Jubiläumsausgabe*, **200**, 85–108.
- Hofbauer, G.** (2012) Jungtertiäre Talverschüttung und tektonische Verstellung entlang des Regnitz-Rezat-Tals. *GdGH Berichte*, **15**, 1–16.
- Hoffmann, M. and Friedrich, A.** (2017) Erosional and tectonic overprint of the mid-Miocene marine cliff line and its applicability as a paleo-geodetic marker of regional-scale tilting, Swabian Alb, southwestern Germany. In: *Young Tectonic Evolution of the Northern Alpine Foreland Basin, Southern Germany, Based on Linking Geomorphology and Structural Geology* (Ed. Hoffmann, M.), pp. 67–110. Ludwig-Maximilians-Universität München, München.
- Holbrook, J.M., Scott, R.W. and Oboh-Ikuenobe, F.E.** (2006) Base-Level Buffers and Buttresses: A Model for Upstream Versus Downstream Control on Fluvial Geometry and Architecture Within Sequences. *J. Sed. Res.*, **76**, 162–174.
- Horwitz, E.P., Chiarizia, R. and Dietz, M.L.** (1992) A novel strontium-selective extraction chromatographic resin. *Solvent Extrac. Ion Exchange*, **10**, 313–336.
- van Houten, F.B.** (1973) Origin of Red Beds. A Review-1961-1972. *Annu. Rev. Earth Planet. Sci.*, **1**, 39–61.
- Hüttner, R. and Schmidt-Kaler, H.** (1999) *Wanderungen in die Erdgeschichte: Meteoritenkrater Nördlinger Ries*. Verlag Dr. Friedrich Pfeil, München.
- Jin, J., Aigner, T., Luterbacher, H., Bachmann, G.H. and Müller, M.** (1995) Sequence stratigraphy and depositional history in the south-eastern German Molasse Basin. *Mar. Petrol. Geol.*, **12**, 929–940.
- Jin, Z., Yu, J., Wang, S., Zhang, F., Shi, Y. and You, C.-F.** (2009) Constraints on water chemistry by chemical weathering in the Lake Qinghai catchment, northeastern Tibetan Plateau (China): clues from Sr and its isotopic geochemistry. *Hydrogeol. J.*, **17**, 2037–2048.
- Kadolsky, D.** (2008) Zur Identität und Synonymie der häufigeren „Hydrobien“ der Rüssingen-Formation (Inflata-Schichten) und Wiesbaden-Formation (Hydrobien-Schichten) (Miozän, Mainzer Becken) (Gastropoda, Prosobranchia: Rissooidea). *Senckenb Lethaea*, **88**, 229–266.
- Knetsch, G.** (1963) *Geologie von Deutschland: und einigen Randgebieten*. Ferdinand Enke Verlag, Stuttgart, 386 pp.
- Koch, P.L., Zachos, J.C. and Dettman, D.L.** (1995) Stable isotope stratigraphy and paleoclimatology of the Paleogene Bighorn Basin (Wyoming, USA). *Palaeogeogr. Palaeoclimatol. Palaeoecol.*, **115**, 61–89.
- Köster, M.H., Hölzl, S. and Gilg, H.A.** (2017) A strontium isotope and trace element geochemical study of dolomite-bearing bentonite deposits in Bavaria (Germany). *Clay Mineral.*, **52**, 161–190.
- Kraus, M.J.** (1987) Integration of channel and floodplain suites; II, Vertical relations of alluvial Paleosols. *J. Sed. Res.*, **57**, 602–612.

- Kraus, M.J.** and **Aslan, A.** (1993) Eocene hydromorphic Paleosols; significance for interpreting ancient floodplain processes. *J. Sed. Res.*, **63**, 453–463.
- Krijgsman, M., Garcés, M., Langereis, C.G., Daams, R., van Dam, J., Meulen, A., van der Augustí, J. and Cabrera, L.** (1996) A new chronology for the middle to late Miocene continental record in Spain. *Earth Planet. Sci. Lett.*, **142**, 367–380.
- Krumbeck, L.** (1926) Über neue und bekannte Tertiärvorkommen in Mittelfranken: Centralblatt für Mineralogie. *Geologie und Paläontologie Abt. B*, **1926**, 33–43.
- Krumbeck, L.** (1927) Zur Kenntnis der alten Schotter des nordbayrischen Deckgebirges: ein Beitrag zur älteren Flußgeschichte Nordbayerns. *Geologische und Paläontologische Abhandlungen, Neue Folge*, **15**, 181–318.
- Last, W.M., Teller, J.T. and Forester, R.M.** (1994) Paleohydrology and paleochemistry of Lake Manitoba, Canada: the isotope and ostracode records. *J. Paleolimnol.*, **12**, 269–282.
- Leeder, M.** (1975) Pedogenic carbonates and flood sediment accretion rates: a quantitative model for alluvial arid-zone lithofacies. *Geol. Mag.*, **112**, 257–270.
- Leeder, M. and Stewart, M.** (1996) Fluvial incision and sequence stratigraphy: alluvial responses to relative sea-level fall and their detection in the geological record. *Geol. Soc. London, Spec. Pub.*, **103**, 25–39.
- Lemcke, K.** (1975) Molasse und vortertiärer Untergrund im Westteil des süddeutschen Alpenvorlandes. *Jahresberichte und Mitteilungen des Oberrheinischen Geologischen Vereins*, 87–115.
- Lemcke, K.** (1985) Flußfracht von Ur-Main und Ur-Naab in der Schweiz und im deutschen Molassebecken. *Bulletin der Vereinigung Schweizerischer Petroleum-Geologen und Ingenieure*, **51**, 13–21.
- Leng, M.J. and Marshall, J.D.** (2004) Palaeoclimate interpretation of stable isotope data from lake sediment archives. *Quatern. Sci. Rev.*, **23**, 811–831.
- Li H.-C., Ku T.-L.** (1997)  $\delta^{13}\text{C}$ – $\delta^{18}\text{C}$  covariance as a paleohydrological indicator for closed-basin lakes. *Palaeogeogr. Palaeoclimatol. Palaeoecol.*, **133**, 69–80. [http://dx.doi.org/10.1016/s0031-0182\(96\)00153-8](http://dx.doi.org/10.1016/s0031-0182(96)00153-8).
- Liu, C., Wang, Z. and Raub, T.D.** (2013) Geochemical constraints on the origin of Marinoan cap dolostones from Nuccaleena Formation, South Australia. *Chem. Geol.*, **351**, 95–104.
- Mack, G.H. and James, W.** (1994) Paleoclimate and the global distribution of paleosols. *J. Geol.*, **102**, 360–366.
- Manzo, E., Perri, E. and Tucker, M.E.** (2012) Carbonate deposition in a fluvial tufa system: processes and products (Corvino Valley – southern Italy). *Sedimentology*, **59**, 553–577.
- Mayer, B. and Schwark, L.** (1999) A 15,000-year stable isotope record from sediments of Lake Steisslingen, Southwest Germany. *Chem. Geol.*, **161**, 315–337.
- Methner, K., Campani, M., Fiebig, J., Löffler, N., Kempf, O. and Mulch, A.** (2020) Middle Miocene long-term continental temperature change in and out of pace with marine climate records. *Scientific Rep.*, **10**, 7989.
- von Meyer, H.** (1834) *Die fossilen Zähne und Knochen und ihre Ablagerungen in der Gegend von Georgensmünd in Bayern*. J.D. Sauerländer, Frankfurt/Main, pp. 1–122.
- Miall, A.D.** (1985) Architectural-element analysis: A new method of facies analysis applied to fluvial deposits. *Earth-Sci. Rev.*, **22**, 261–308.
- Miall, A.D.** (1996) *The Geology of Fluvial Deposits: Sedimentary Facies, Basin Analysis, and Petroleum Geology*. Springer, Berlin, Heidelberg.
- Newell, A.J., Tverdokhlebov, V.P. and Benton, M.J.** (1999) Interplay of tectonics and climate on a transverse fluvial system, Upper Permian, Southern Uralian Foreland Basin, Russia. *Sed. Geol.*, **127**, 11–29.
- Olsen, P.E.** (1986) A 40-million-year lake record of early Mesozoic orbital climatic forcing. *Science*, **234**, 842–848.
- Opluštil, S., Lojka, R., Rosenau, N.A., Strnad, L. and Sýkorová, I.** (2015) Middle Moscovian climate of eastern equatorial Pangea recorded in paleosols and fluvial architecture. *Palaeogeogr. Palaeoclimatol. Palaeoecol.*, **440**, 328–352.
- Paul, J., Wemmer, K. and Ahrendt, H.** (2008) Provenance of siliciclastic sediments (Permian to Jurassic) in the Central European Basin. *Zeitschrift der Deutschen Gesellschaft für Geowissenschaften*, **159**, 641–650.
- Paul, J., Wemmer, K. and Wetzel, F.** (2009) Keuper (Late Triassic) sediments in Germany—indicators of rapid uplift of Caledonian rocks in southern Norway. *Norwegian J. Geol.*, **89**, 193–202.
- Perri, E., Manzo, E. and Tucker, M.E.** (2012) Multi-scale study of the role of the biofilm in the formation of minerals and fabrics in calcareous tufa. *Sediment. Geol.*, **263–264**, 16–29.
- Peterek, A. and Schröder, B.** (2010) Geomorphologic evolution of the cuesta landscapes around the Northern Franconian Alb—review and synthesis. *Zeitschrift für Geomorphologie*, **54**, 305–345.
- Pietzsch, R., Oliveira, D.M., Tedeschi, L.R., Queiroz Neto, J.V., Figueiredo, M.F., Vazquez, J.C. and de Souza, R.S.** (2018) Palaeohydrology of the Lower Cretaceous pre-salt lacustrine system, from rift to post-rift phase, Santos Basin, Brazil. *Palaeogeogr. Palaeoclimatol. Palaeoecol.*, **507**, 60–80.
- Piller, W.E., Harzhauser, M. & Mandic, O.** (2007) Miocene Central Paratethys stratigraphy—current status and future directions. *Stratigraphy*, **4**, 151–168.
- Pin, C. and Bassin, C.** (1992) Evaluation of a strontium-specific extraction chromatographic method for isotopic analysis in geological materials. *Anal. Chim. Acta*, **269**, 249–255.
- Pippèrr, M. and Reichenbacher, B.** (2017) Late Early Miocene palaeoenvironmental changes in the North Alpine Foreland Basin. *Palaeogeogr. Palaeoclimatol. Palaeoecol.*, **468**, 485–502.
- Pla-Pueyo, S., Gierlowski-Kordesch, E.H., Viseras, C. and Soria, J.M.** (2009) Major controls on sedimentation during the evolution of a continental basin: Pliocene-Pleistocene of the Guadix Basin (Betic Cordillera, southern Spain). *Sed. Geol.*, **219**, 97–114.
- Platt, N.H. and Wright, V.P.** (1992) Palustrine carbonates and the Florida Everglades; towards an exposure index for the fresh-water environment? *J. Sed. Res.*, **62**, 1058–1071.
- Pohl, J., Stoeffler, D. and Gall, H.V. and Ernstson, K.** (1977) The Ries impact crater. In: *Impact and Explosion Cratering: Planetary and Terrestrial Implications* (Eds Roddy, D. J., Pepin, R. P. and Merrill, R. B.), pp. 343–404. Pergamon, New York.
- Polissar, P.J., Freeman, K.H., Rowley, D.B., McInerney, F.A. and Currie, B.S.** (2009) Paleoaltimetry of the Tibetan Plateau from D/H ratios of lipid biomarkers. *Earth Planet. Sci. Lett.*, **287**, 64–76.
- Quade, J., Cerling, T.E. and Bowman, J.R.** (1989) Systematic variations in the carbon and oxygen isotopic composition

- of pedogenic carbonate along elevation transects in the southern Great Basin, United States. *Geol. Soc. Am. Bull.*, **101**, 464–475.
- Reading, H.G.** (1996) *Sedimentary Environments: Processes, Facies and Stratigraphy*, 3rd edn. Wiley-Blackwell, Oxford, 704 pp.
- Reck, H.** (1912) Die morphologische Entwicklung der süddeutschen Schichtstufenlandschaft im Lichte der Davis' schen Cyclustheorie. *Zeitschrift der Deutschen Geologischen Gesellschaft*, 81–232.
- Reichenbacher, B., Krijgsman, W., Lataster, Y., Pippèr, M., Van Baak, C.G., Chang, L., Kälin, D., Jost, J., Doppler, G. and Jung, D.** (2013) A new magnetostratigraphic framework for the lower Miocene (Burdigalian/Ottungian, Karpatian) in the North Alpine Foreland Basin. *Swiss J. Geosci.*, **106**, 309–334.
- Reuter, L.** (1927) Geologische Darstellung des schwäbisch-fränkischen Juras, seines triadischen Vorlandes und des südlich angrenzenden Molasse-Gebietes. In: *Abriß der Geologie von Bayern r.d.Rh. in sechs Abteilungen, Abteilung IV* (Ed. Schuster, M.), Oldenbourg und Piloty & Loehle, Munich, 166 pp.
- Rhodes, M.K., Carroll, A.R., Pietras, J.T., Beard, B.L. and Johnson, C.M.** (2002) Strontium isotope record of paleohydrology and continental weathering, Eocene Green River Formation, Wyoming. *Geology*, **30**, 167–170.
- Rocholl, A., Schaltegger, U., Gilg, H.A., Wijbrans, J. and Böhme, M.** (2018a) The age of volcanic tuffs from the Upper Freshwater Molasse (North Alpine Foreland Basin) and their possible use for tephrostratigraphic correlations across Europe for the Middle Miocene. *Int. J. Earth Sci.*, **107**, 387–407.
- Rocholl, A., Böhme, M., Gilg, H.A., Pohl, J., Schaltegger, U. and Wijbrans, J.** (2018b) Comment on “A high-precision  $^{40}\text{Ar}/^{39}\text{Ar}$  age for the Nördlinger Ries impact crater, Germany, and implications for the accurate dating of terrestrial impact events” by Schmieder et al. (*Geochim. Cosmochim. Acta* 220 (2018) 146–157). *Geochim. Cosmochim. Acta*, **238**, 599–601.
- Rowley, D.B. and Garzone, C.N.** (2007) Stable isotope-based paleoaltimetry. *Annu. Rev. Earth Planet. Sci.*, **35**, 463–508.
- Ruf, M., Link, E., Pross, J. and Aigner, T.** (2005) Integrated sequence stratigraphy: Facies, stable isotope and palynofacies analysis in a deeper epicontinental carbonate ramp (Late Jurassic, SW Germany). *Sed. Geol.*, **175**, 391–414.
- Rust, B.R.** (1982) Sedimentation in fluvial and lacustrine environments. In: *Sediment/Freshwater Interaction* (Ed. Sly, P.G.). *Developments in Hydrobiology*, **9**, pp. 59–70.
- Sant, K., Kirscher, U., Reichenbacher, B., Pippèr, M., Jung, D., Doppler, G. and Krijgsman, W.** (2017) Late Burdigalian sea retreat from the North Alpine Foreland Basin: new magnetostratigraphic age constraints. *Global Planet. Change*, **152**, 38–50.
- Schirmer, W.** (2014) Moenodanuvius-Flussweg quer durch Franken. *Natur und Mensch, Jahresmitteilungen der Naturhistorischen Gesellschaft Nürnberg*, **2013**, 89–146.
- Schmieder, M., Kennedy, T., Jourdan, F., Buchner, E. and Reimold, W.U.** (2018a) A high-precision  $^{40}\text{Ar}/^{39}\text{Ar}$  age for the Nördlinger Ries impact crater, Germany, and implications for the accurate dating of terrestrial impact events. *Geochim. Cosmochim. Acta*, **220**, 146–157.
- Schmieder, M., Kennedy, T., Jourdan, F., Buchner, E. and Reimold, W.U.** (2018b) Response to comment on “A high-precision  $^{40}\text{Ar}/^{39}\text{Ar}$  age for the Nördlinger Ries impact crater, Germany, and implications for the accurate dating of terrestrial impact events” by Schmieder et al. (*Geochim. Cosmochim. Acta*, **238**, 602–605). *Geochim. Cosmochim. Acta*, **238**, 602–605.
- Schumm, S.A.** (1985) Patterns of alluvial rivers. *Annu. Rev. Earth Planet. Sci.*, **13**, 5–27.
- Schumm, S.A.** (1993) River Response to Baselevel Change: Implications for Sequence Stratigraphy. *J. Geol.*, **101**, 279–294.
- Selley, R.C.** (1992). *Ancient Sedimentary Environments and Their Sub-Surface Diagnosis*. 3rd edn., repr. Chapman and Hall, London.
- Semeniuk, V. and Meagher, T.D.** (1981) Calcrete in Quaternary coastal dunes in southwestern Australia; a capillary-rise phenomenon associated with plants. *J. Sed. Res.*, **51**, 47–68.
- Sheldon, N.D.** (2005) Do red beds indicate paleoclimatic conditions?: a Permian case study. *Palaeogeogr. Palaeoclimatol. Palaeoecol.*, **228**, 305–319.
- Shoemaker, E.M. and Chao, E.C.** (1961) New evidence for the impact origin of the Ries Basin, Bavaria, Germany. *J. Geophys. Res.*, **66**, 3371–3378.
- Shukla, U., Bachmann, G., Beutler, G., Barnasch, J. and Franz, M.** (2006) Extremely distal fluvial sandstone within the playa system of Arnstadt Formation (Norian, Late Triassic), Central Germany. *Facies*, **52**, 541–554.
- Song, B., Zhang, K., Zhang, L., Ji, J., Hong, H., Wei, Y., Xu, Y., Algeo, T.J. and Wang, C.** (2018) Qaidam Basin paleosols reflect climate and weathering intensity on the northeastern Tibetan Plateau during the Early Eocene Climatic Optimum. *Palaeogeogr. Palaeoclimatol. Palaeoecol.*, **512**, 6–22.
- Staisch, L.M., Niemi, N.A., Hong, C., Clark, M.K., Rowley, D.B. and Currie, B.** (2014) A Cretaceous-Eocene depositional age for the Fenghuoshan Group, Hoh Xil Basin: Implications for the tectonic evolution of the northern Tibet Plateau. *Tectonics*, **33**, 281–301.
- Stevenson, F.** (1969) Pedohumus: accumulation and diagenesis during the Quaternary. *Soil Sci.*, **107**, 470–479.
- Sturm, S., Kenkmann, T., Willmes, M., Pösges, G. and Hiesinger, H.** (2015) The distribution of megablocks in the Ries crater, Germany: Remote sensing, field investigation, and statistical analyses. *Meteorit. Planet. Sci.*, **50**, 141–171.
- Swart, P.K.** (2015) The geochemistry of carbonate diagenesis: The past, present and future. *Sedimentology*, **62**, 1233–1304.
- Talbot, M.** (1990) A review of the palaeohydrological interpretation of carbon and oxygen isotopic ratios in primary lacustrine carbonates. *Chem. Geol. Isotope Geosci. Sec.*, **80**, 261–279.
- Talbot, M. and Kelts, K.** (1986) Primary and diagenetic carbonates in the anoxic sediments of Lake Bosumtwi, Ghana. *Geology*, **14**, 912–916.
- Tandon, S. and Gibling, M.** (1994) Calcrete and coal in late Carboniferous cyclothems of Nova Scotia, Canada: Climate and sea-level changes linked. *Geology*, **22**, 755–758.
- Tanner, L.H.** (2010) Continental carbonates as indicators of paleoclimate. In: *Developments in Sedimentology*, Vol. **62** (Eds Alonso-Zarza, A.M. and Tanner, L.H.), pp. 179–214. Elsevier, The Netherlands.
- Thompson, J.B., Schultze-Lam, S., Beveridge, T.J. and Des Marais, D.J.** (1997) Whiting events: Biogenic origin due to the photosynthetic activity of cyanobacterial picoplankton. *Limnol. Oceanogr.*, **42**, 133–141.
- Tütken, T., Vennemann, T., Janz, H. and Heizmann, E.** (2006) Palaeoenvironment and palaeoclimate of the

- Middle Miocene lake in the Steinheim basin, SW Germany: a reconstruction from C, O, and Sr isotopes of fossil remains. *Palaeogeogr. Palaeoclimatol. Palaeoecol.*, **241**, 457–491.
- Ufrecht, W.** and **Hölzl, S.** (2006) Salinare Mineral- und Thermalwässer im Oberen Muschelkalk (Trias) im Großraum Stuttgart-Rückschlüsse auf Herkunft und Entstehung mit Hilfe der  $^{87}\text{Sr}/^{86}\text{Sr}$ -Strontium-Isotopie [Saline waters in the Upper Muschelkalk Aquifer (Triassic) in the area of Stuttgart-conclusions to origin and evolution by means of  $^{87}\text{Sr}/^{86}\text{Sr}$ -strontium isotopes]. *Zeitschrift der deutschen Gesellschaft für Geowissenschaften*, **157**, 299–315.
- Utrilla, R., Vázquez, A.** and **Anadón, P.** (1998) Paleohydrology of the Upper Miocene Bicorn Lake (eastern Spain) as inferred from stable isotopic data from inorganic carbonates. *Sed. Geol.*, **121**, 191–206.
- Valero Garcés, B.L., Moreno, A., Navas, A., Mata, P., Machín, J., Delgado Huertas, A., González Sampériz, P., Schwalb, A., Morellón, M., Cheng, H. and Edwards, R.L.** (2008) The Taravilla lake and tufa deposits (Central Iberian Range, Spain) as palaeohydrological and palaeoclimatic indicators. *Palaeogeogr. Palaeoclimatol. Palaeoecol.*, **259**, 136–156.
- Vázquez-Urbez, M., Arenas, C. and Pardo, G.** (2012) A sedimentary facies model for stepped, fluvial tufa systems in the Iberian Range (Spain): the Quaternary Piedra and Mesa valleys. *Sedimentology*, **59**, 502–526.
- Veizer, J.** (1989) Strontium isotopes in seawater through time. *Palaeogeogr. Palaeoclimatol. Palaeoecol.*, **17**, 141–167.
- Veizer, J., Ala, D., Azmy, K., Bruckschen, P., Buhl, D., Bruhn, F., Carden, G.A., Diener, A., Ebner, S. and Godderis, Y.** (1999)  $^{87}\text{Sr}/^{86}\text{Sr}$ ,  $\delta^{13}\text{C}$  and  $\delta^{18}\text{O}$  evolution of Phanerozoic seawater. *Chem. Geol.*, **161**, 59–88.
- Wagner, G.** (1923) *Aus der Geschichte der Altmühl*. Fränkische Heimat-Schriften, Spindler, Nürnberg, 116 pp.
- Wagner, G.** (1960) *Einführung in die Erd- und Landschaftsgeschichte: mit besonderer Berücksichtigung Süddeutschlands*. Ferdinand Rau, Öhringen, 622 + 176 pp.
- Weiss, C., Höfling, R. and Lorenz, H.G.** (2008) Die Fazies lakustriner und palustriner Karbonate aus dem Miozän von Langenaltheim/Südliche Frankenalb. *Jahresberichte und Mitteilungen des Oberrheinischen Geologischen Vereins*, **90**, 73–90.
- Whiticar, M.J.** (1999) Carbon and hydrogen isotope systematics of bacterial formation and oxidation of methane. *Chem. Geol.*, **161**, 291–314.
- Wierzbowski, H., Anczkiewicz, R., Pawlak, J., Rogov, M.A. and Kuznetsov, A.B.** (2017) Revised middle–upper Jurassic strontium isotope stratigraphy. *Chem. Geol.*, **466**, 239–255.
- Wright, V.P. and Marriott, S.B.** (1993) The sequence stratigraphy of fluvial depositional systems: the role of floodplain sediment storage. *Sed. Geol.*, **86**, 203–210.
- Wright, V.P., Platt, N.H. and Wimbledon, W.** (1988) Biogenic laminar calcretes: evidence of calcified root-mat horizons in paleosols. *Sedimentology*, **35**, 603–620.
- Yan, Y., Zhou, J., He, Z., Sun, Q., Fei, J., Zhou, X., Zhao, K., Yang, L., Long, H. and Zheng, H.** (2017) Evolution of Luyang Lake since the last 34,000 years: Climatic changes and anthropogenic impacts. *Quatern. Int.*, **440**, 90–98.
- Zachos, J., Pagani, M., Sloan, L., Thomas, E. and Billups, K.** (2001) Trends, rhythms, and aberrations in global climate 65 Ma to present. *Science*, **292**, 686–693.
- Zieliński, M., Dopieralska, J., Belka, Z., Walczak, A., Siepak, M. and Jakubowicz, M.** (2018) Strontium isotope identification of water mixing and recharge sources in a river system (Oder River, central Europe): A quantitative approach. *Hydrol. Process.*, **32**, 2597–2611.
- Zweigel, J., Aigner, T. and Luterbacher, H.** (1998) Eustatic versus tectonic controls on Alpine foreland basin fill: sequence stratigraphy and subsidence analysis in the SE German Molasse. *Geol. Soc., London, Spec. Pub.*, **134**, 299.

Manuscript received 25 December 2020; revision accepted 30 March 2021

## Supporting Information

Additional information may be found in the online version of this article:

**Fig S1.** Covariation plot of silicate content and  $^{87}\text{Sr}/^{86}\text{Sr}$  of the carbonate samples (6N HCl) of the Miocene Georgensgmünd Formation. From LFT 4 to 9 there is a general increase in the carbonate content.

**Table S1.** Comparison of strontium isotope results of acetic acid and HCl treatments.

**Table S2.** Reference data for stable carbon and oxygen isotopes.